IET Communications

Research Article

IET Journals
The Institution of Engineering and Technology

Precoded generalised frequency division multiplexing system to combat inter-carrier interference: performance analysis

ISSN 1751-8628
Received on 23rd January 2015
Revised on 4th May 2015
Accepted on 31st May 2015
doi: 10.1049/iet-com.2015.0081
www.ietdl.org

Shashank Tiwari[1] ✉, *Suvra Sekhar Das*[1,2], *Kalyan Kumar Bandyopadhyay*[2]

[1]*G.S. Sanyal School of Telecommunications, Indian Institute of Technology, Kharagpur, India*
[2]*Department of Electrical and Electronics Communication, Indian Institute of Technology, Kharagpur, India*
✉ *E-mail: shashank@gssst.iitkgp.ernet.in.*

Abstract: The expected operating scenarios of fifth-generation (5G) pose a great challenge to orthogonal frequency division multiplexing which has poor out of band spectral properties, stringent synchronisation requirements and large symbol duration. Generalised frequency division multiplexing (GFDM) which is the focus of this work has been suggested in the literature as one of the possible solutions to meet 5G requirements. In this study, the analytical performance evaluation of minimum mean square error (MMSE) receiver for GFDM is presented. The authors also proposed precoding techniques to enhance the performance of GFDM. A simplified expression of signal-to-interference and noise ratio (SINR) for MMSE receiver of GFDM is derived using special properties related to the modulation matrix of GFDM, which are described in this study. This SINR is used to evaluate the bit error rate performance. Precoding schemes are proposed to reduce complexity of GFDM–MMSE receiver without compromising on the performance. Block inverse discrete Fourier transform (BIDFT) and discrete Fourier transform (DFT)-based precoding schemes are found to outperform GFDM–MMSE receiver due to frequency diversity gain while having complexity similar to zero-forcing receiver of GFDM. It is shown that both BIDFT- and DFT-based precoding schemes reduce peak-to-average power ratio significantly. Computational complexities of different transmitters and receivers of precoded and uncoded GFDM are also presented.

1 Introduction

The need for wireless links, from proximity to a large distance communication, has been on the rise since its origin without ever showing any signs of distaste to growth. Toward this, several applications with diverse needs have driven the development of technical solutions. Amongst many, the domain of public wireless communication has provided one of the greatest benefits and drive to the development of society. The success is powered by standardisation, which led to mass production and adoption of technology due to cost effectiveness. The developments of 1G–4G [1, 2] have fundamental drivers as the 'need for speed' (higher data rate and higher spectral efficiency) and the requirement of lower latency. The next generation, fifth generation (5G) is also expected to be driven by similar demands but with added needs such as flexibility. Some of the important applications operating 5G [3–6] are flexible radio (cognitive radio), tactile internet (TI), machine type communication (MTC), great service in crowd, super real-time services, super reliable communication and others. Orthogonal frequency division multiplexing (OFDM) is de-facto transmission technology for broadband wireless access due to the robustness to multipath fading, high spectral efficiency and ease of implementation but has limited capability in meeting the needs of new requirements of 5G [7, 8]. MTC demands relaxed synchronisation requirement which is a limitation in OFDM as it is sensitive to frequency errors. Small symbol duration is needed for low-latency applications and due to the cyclic prefix (CP), OFDM will lead to low efficiency. High out of band (OoB) radiation of OFDM limits, its use for opportunistic use of spectrum and dynamic spectrum allocation.

To meet above requirements, filter bank multi-carrier (FBMC) [9–12], constant envelope-OFDM [13], generalised frequency division multiplexing (GFDM) [14], unified filtered multi-carrier (UFMC) [15] have been proposed, where each has its own special features. FBMC, whose concept dates back to 1967 [16], is currently being considered as a candidate for 5G waveform due to its good frequency localisation capabilities as well as low OoB radiation. However, FBMC signal suffers from inter-symbol interference as no CP is used. The FBMC signal stretches in time, and hence limits spectral efficiency gains. Hence, FBMC is not suitable for low-latency applications [17]. UFMC (proposed for low-latency applications) has limited suppression of OoB radiation. In this paper, we focus on GFDM, which is another competitive waveform. GFDM has been shown to be flexible [3, 18, 19] in terms of using time–frequency resources. It has good OoB radiation properties [20]. It is also quite resilient to synchronisation requirement [19] and has good spectral efficiency as it uses circular pulse shaping which reduces CP length in frequency selective fading channel (FSFC).

Although GFDM has attractive features, yet there remain sufficient investigations to be done before it can be adopted into practical communication systems. One of the fundamental differences between GFDM and OFDM is that the former uses non-rectangular pulse shape on each subcarrier where it was rectangular for the latter. This causes inter-carrier interference (ICI) [21]. Therefore, receiver design is an important issue in GFDM. It was earlier quite simple in the case of OFDM which led to its mass adoption. GFDM receiver in FSFC has been proposed as a two-stage receiver [22]. Frequency-domain zero-forcing (ZF) equalisation is used to mitigate the effect of the wireless channel in the first stage [19]. In the second stage, linear as well as non-linear receivers have been proposed to mitigate self-interference in GFDM systems [23, 24]. Linear receivers of GFDM such as matched filter (MF), ZF and minimum mean square error (MMSE) are proposed in [23]. It has been shown that MF is not able to mitigate self-interference. It has also been shown in [22, 23] that MMSE performs better than ZF, especially when signal-to-interference and noise ratio (SINR) is low. For high SINR, MMSE performance matches with ZF. Analytical expression for bit error rate (BER) for MF and ZF receivers over

© The Institution of Engineering and Technology 2015

additive white Gaussian noise (AWGN) channel is given in [19, 20]. Analytical expression of SINR is an essential part of performance analysis of a system as it leads to the calculation of error probability and capacity. BER computation for MMSE receiver is still not available in the literature.

Since implementation of MMSE receiver requires very high amount of complexity, successive interference cancellation (SIC) receivers to mitigate self-interference in AWGN channel were proposed in [24]. Double-SIC (D-SIC) receiver introduced in [24] cancels interference from two adjacent subcarriers of all symbols. D-SIC can cancel out self-interference entirely in AWGN channel but requires few iterations thus induce processing delay at the receiver. For usability of GFDM, low-complexity signal processing techniques remain to be investigated.

Peak-to-average power ratio (PAPR) is an important issue in the multi-carrier communication. We expect GFDM to have a higher PAPR than OFDM as the use of identical non-rectangular pulse shapes increase PAPR in multi-carrier system [25]. Michailow and Fettweis [26] have compared PAPR of GFDM with OFDM for unequal number of subcarriers. As far as we know, PAPR comparison of GFDM with OFDM for equal number of subcarriers has not been investigated. Apart from that PAPR reduction schemes also need to be studied.

A detailed exposition of the product of the modulation matrix with its Hermitian reveals some interesting properties which help in performance analysis and developing precoding techniques. The details are described in this paper. A simplified expression for SINR of MMSE receiver is developed using the above-mentioned special properties. It is also shown that interference plus noise values can be approximated as a Gaussian random variable. Analytical BER is computed in AWGN and FSFC using derived SINR expressions.

A detailed complexity analysis of different schemes is presented in this paper which shows that D-SIC is not quite simple to implement in comparison with ZF receiver. To reduce the self-interference at the receiver, precoding techniques for GFDM are investigated in this paper. A generalised framework for precoding-based GFDM is developed. On the basis of the properties related to the modulation matrix as mentioned above, block inverse discrete Fourier transform (BIDFT)-based precoding is proposed. Performance of BIDFT, discrete Fourier transform (DFT) and singular value decomposition (SVD)-based precoding techniques are compared with uncoded GFDM. PAPR of precoded GFDM is compared with uncoded GFDM and OFDM as well.

The rest of this paper is organised as follows. The system model is developed in Section 2. Analytical BER for MMSE receiver is presented in Section 3. The precoding schemes proposed in this paper are presented in Section 4. Results related to the proposed works are given in Section 5. Section 6 has the conclusion.

In this paper, vectors are represented by bold small letters, matrices are represented by bold capital letters and scalars are represented as normal small letters. The operation $a(n \bmod l)$ is written as $a(n)_l$, $\boldsymbol{I}_N$ represents identity matrix with order N and '*' represents convolution operation. E is expectation operation and $j = \sqrt{-1}$.

2 System model

GFDM is a multi-carrier modulation technique with some similarity to OFDM. We begin by considering a block of quadrature amplitude modulation (QAM) modulated symbols $\boldsymbol{d} = [d_0 d_1 \cdots d_{MN-1}]^{\mathrm{T}}$. We assume that data symbols are independent and identical, that is, $E[d_l d_l^*] = \sigma_d^2$, $\forall l$ and $E[d_l d_q^*] = 0$ when $l \neq q$. Let the total bandwidth B be divided into N number of subcarriers where symbol duration $T = N/B$ second and B/N Hz is the subcarrier bandwidth. In case of OFDM this leads to orthogonal subcarriers. Let the symbol duration, T, be one time slot. GFDM is a block-based transmission scheme and we consider a block to have M such time slots. Hence, in one block there are N subcarriers $\times M$ timeslots $= NM$ QAM symbols. The flow of operations, as described below, can be understood in the light of Fig. 1.

2.1 Transmitter

Since we consider precoding, let $\boldsymbol{P}$ be a precoding matrix of size $MN \times MN$, which is defined in Section 4. The data vector $\boldsymbol{d}$ be multiplied with precoding matrix $\boldsymbol{P}$ and we obtain precoded data vector $\tilde{\boldsymbol{d}} = \boldsymbol{P}\boldsymbol{d}$. The $MN \times 1$ precoded data vector $\tilde{\boldsymbol{d}} = [\tilde{d}_{0,0} \cdots \tilde{d}_{k,m} \cdots \tilde{d}_{N-1,M-1}]^{\mathrm{T}}$, where $k = 0 \cdots N-1$ denote subcarrier index and $m = 0 \cdots M-1$ indicates time slot index. Conventional GFDM system [19] can be seen as a special case of precoded GFDM system when $\boldsymbol{P} = \boldsymbol{I}_{NM}$. The precoded data vector, $\tilde{\boldsymbol{d}}$, is modulated using GFDM modulator. Precoded data $\tilde{d}_{k,m}$ is first upsampled by N, which is represented as

$$\tilde{d}^{\mathrm{up}}_{k,m}(n) = \tilde{d}_{k,m}\delta(n - mN), \quad n = 0,\ 1,\ \ldots,\ MN-1. \tag{1}$$

Now, this upsampled data is pulse shaped. Impulse response of pulse shaping filter is represented by $g(n)$. Its length is MN. The upsampled precoded data $\tilde{d}^{\mathrm{up}}_{k,m(n)}$ is circularly convoluted with such pulse shaping filter $g(n)$ and can be written as

$$\begin{aligned} x^f_{k,m}(n) &= \sum_{r=0}^{MN-1} \tilde{d}_{k,m} g(n-r)_{MN}\delta(r - mN) \\ &= \tilde{d}_{k,m} g(n - mN)_{MN}. \end{aligned} \tag{2}$$

Now the filtered data is up-converted to kth subcarrier frequency and is given as,

$$x_{k,m}(n) = \tilde{d}_{k,m} g(n - mN)_{MN} \mathrm{e}^{\mathrm{j}2\pi kn/N} = \tilde{d}_{k,m} a_{k,m}(n), \tag{3}$$

where $a_{k,m}(n) = g(n - mN)_{MN}\mathrm{e}^{\mathrm{j}2\pi kn/N}$ for $n = 0,\ 1,\ \ldots,\ MN-1$ is called the kernel of GFDM for the kth subcarrier and the mth time slot. Now, output samples of all subcarrier frequencies and time slots are added and the GFDM signal can be given as,

$$x(n) = \sum_{m=0}^{M-1}\sum_{k=0}^{N-1} x_{k,m}(n) = \sum_{m=0}^{M-1}\sum_{k=0}^{N-1} \tilde{d}_{k,m} a_{k,m}(n). \tag{4}$$

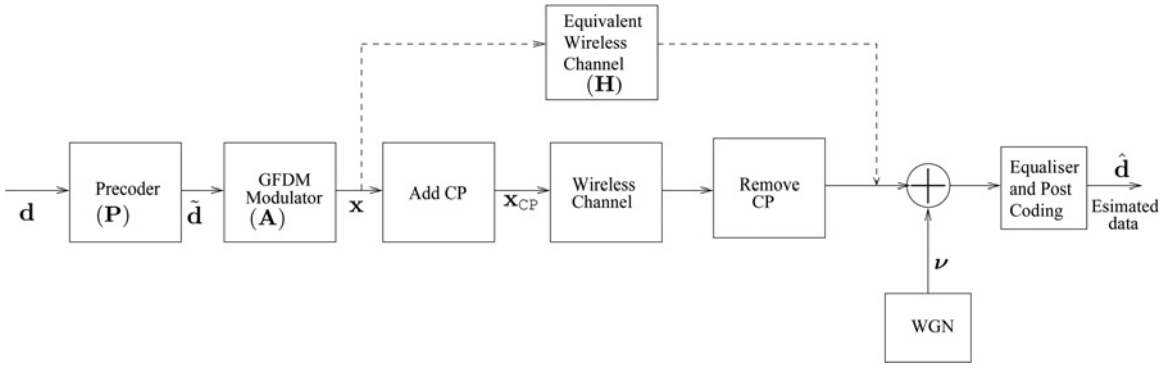

Fig. 1 *Transmitter and receiver architecture for precoding-based GFDM system*

IET Commun., 2015, Vol. 9, Iss. 15, pp. 1829–1841
© The Institution of Engineering and Technology 2015

If we let, $l = mN + k$ for $m = 0, 1, \ldots, M-1$ and $k = 0, 1, \ldots, N-1$. Then, we may write (4) as,

$$x(n) = \sum_{l=0}^{MN-1} a_l^N(n)\tilde{d}_l^N, \tag{5}$$

where superscript N is the identifier of the specific mapping between index l and time slot and subcarrier index tuple (k, m) which takes N as scalar multiplier in the mapping. If we collect all output samples of GFDM signal in a vector called $\boldsymbol{x} = [x(0)x(1)\cdots x(MN-1)]^{\mathrm{T}}$ and all samples of $a_l^N(n)$ is a vector called $\boldsymbol{a}_l^N = [a_l^N(0)a_l^N(1)\cdots a_l^N(MN-1)]$. Then using (5), $\boldsymbol{x}$ can be written as,

$$\boldsymbol{x} = \sum_{l=0}^{MN-1} \boldsymbol{a}_l^N\tilde{d}_l^N \equiv \sum_{l=0}^{MN-1} \tilde{d}_l^N \times l^{\text{th}} \text{ column vector } \boldsymbol{a}_l^N = \boldsymbol{A}_N\tilde{\boldsymbol{d}}^N, \tag{6}$$

where $\boldsymbol{A}_N = [\boldsymbol{a}_0^N\boldsymbol{a}_1^N\cdots\boldsymbol{a}_{MN-1}^N]$ is the modulation matrix, $\tilde{\boldsymbol{d}}^N = [\tilde{d}_0\tilde{d}_1\cdots\tilde{d}_l\cdots\tilde{d}_{NM-1}]^{\mathrm{T}}$ is the precoded data vector. If we collect all samples of $a_{k,\ m}(n)$ is the vector called $\boldsymbol{a}_{k,m} = [a_{k,m}(0)a_{k,m}(0)\cdots a_{k,m}(MN-1)]^{\mathrm{T}}$, then $\boldsymbol{A}_N$ can also be written as, (see (7)). Where $\rho = \mathrm{e}^{\mathrm{j}2\pi/N}$. At this point, it is also interesting to look into the structure $\boldsymbol{a}_{k,\ m}$ vectors which constitute columns of $\boldsymbol{A}_N$. The first column of $\boldsymbol{A}_N$, that is, $\boldsymbol{a}_{0,0}$ holds all coefficients of pulse shaping filter and other columns of $\boldsymbol{A}_N$ or other vectors in the set of $\boldsymbol{a}_{k,\ m}$'s are time and frequency shifted versions of $\boldsymbol{a}_{0,0}$ where frequency index k denotes k/N shift in frequency and time index m denotes m time slot or mN sample cyclic shift. Taking clue from description of column vectors $\boldsymbol{a}_{k,\ m}$, structure of $\boldsymbol{A}_N$ can be understood by (7). Columns having same time shift are put together. Columns which are N column index apart are time shifted versions of each other. Columns having same time shift are arranged in increasing order of frequency shift. We will explore time-domain and frequency-domain behaviour for an example $\boldsymbol{A}_N$ with total subcarriers $N = 4$ and total time slots $M = 5$. Pulse shaping filter is taken to be root raised cosine (RRC) with roll of factor (ROF) of 0.9. Fig. 2 shows the absolute values of each column index $u = 0, 1, \ldots, MN-1$ with sample index $n =$ 0, 1, …, $MN-1$. It can be observed that first $N = 4$ columns have 0 time shift and next N columns have unit time shift and so on.

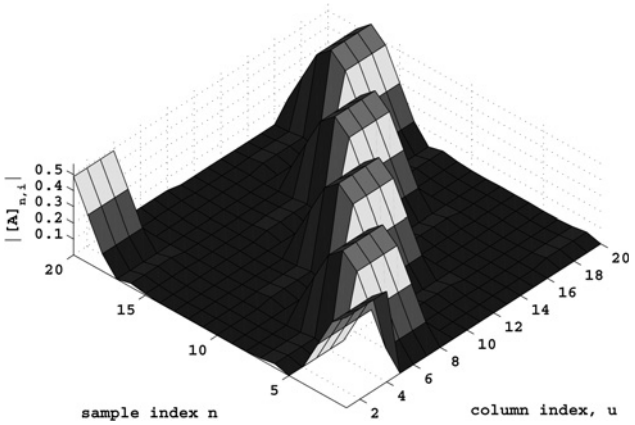

Fig. 2 *Time-domain view of columns of $\boldsymbol{A}$ for $N = 4$, $M = 5$ and ROF = 0.9*

Alternatively, if we take $l = kM + m$ in (4), modulation matrix $\boldsymbol{A}_M$ can be represented as, (see (8)). Matrixes $\boldsymbol{A}_N$ and $\boldsymbol{A}_M$ can be related as $\boldsymbol{A}_N = \boldsymbol{\zeta}\boldsymbol{A}_M$, where $\boldsymbol{\zeta}$ is a permutation matrix which permutes column of matrix applied. CP is added to GFDM modulated block to prevent inter-block interference in FSFC. CP of length N_{CP} is prepended to $\boldsymbol{x}$. After adding CP, transmitted vector, $\boldsymbol{x}_{\mathrm{cp}}$, can be given as

$$\boldsymbol{x}_{\mathrm{cp}} = [\boldsymbol{x}(MN - N_{\mathrm{cp}} + 1{:}MN);\ \boldsymbol{x}] \tag{9}$$

In the rest of this paper, for equations which are valid for both $\boldsymbol{A}_M$ and $\boldsymbol{A}_N$, modulation matrix will be denoted as $\boldsymbol{A}$. However, wherever required $\boldsymbol{A}_N$ and $\boldsymbol{A}_M$ will be specified.

2.2 Receiver

Let, $\boldsymbol{h} = [h_1, h_2, \ldots, h_L]^{\mathrm{T}}$ be the L length channel impulse response vector, where, h_r, for $1 \le r \le L$, represents the complex baseband

$$\boldsymbol{A}_N = [\underbrace{\overbrace{\boldsymbol{a}_{0,0}}^{\text{1st freq.}}\ \overbrace{\boldsymbol{a}_{1,0}}^{\text{2nd freq.}}\ \cdots\ \overbrace{\boldsymbol{a}_{N-1,0}}^{N\text{th freq.}}}_{\text{1st time slot}} | \underbrace{\boldsymbol{a}_{0,1}\boldsymbol{a}_{1,1}\cdots\boldsymbol{a}_{N-1,1}}_{\text{2nd time slot}} | \cdots | \underbrace{\boldsymbol{a}_{0,M-1}\boldsymbol{a}_{1,M-1}\cdots\boldsymbol{a}_{N-1,M-1}}_{M\text{th time slot}}]$$

$$= \begin{bmatrix} g(0) & g(0) & \cdots & \cdots & g(0) \\ g(1) & g(1)\rho & \cdots & \cdots & g(1)\rho^{N-1} \\ \vdots & \vdots & \cdots & \cdots & \vdots \\ \vdots & \vdots & \cdots & \cdots & \vdots \\ \underbrace{g(MN-1)}_{\boldsymbol{a}_{0,0}} & \underbrace{g(MN-1)\rho^{MN-1}}_{\boldsymbol{a}_{1,0}} & \cdots & \cdots & \underbrace{g(MN-1)\rho^{(N-1)(MN-1)}}_{\boldsymbol{a}_{N-1,0}} \end{bmatrix} \tag{7}$$

$$\begin{bmatrix} g(MN-N) & \cdots & \cdots & g(MN-N) & \cdots \\ g(MN-N+1) & \cdots & \cdots & g(MN-N+1)\rho^{N-1} & \vdots \\ \vdots & \cdots & \cdots & \vdots & (M-2)N \text{ terms} \\ \vdots & \cdots & \cdots & \vdots & \vdots \\ \underbrace{g(MN-N-1)}_{\boldsymbol{a}_{0,1}} & \cdots & \cdots & \underbrace{g(MN-N-1)\rho^{(N-1)(MN-1)}}_{\boldsymbol{a}_{N-1,1}} & \cdots \end{bmatrix},$$

$$\boldsymbol{A}_M = [\underbrace{\overbrace{\boldsymbol{a}_{0,0}}^{\substack{1\text{st}\\ \text{time}}}\ \overbrace{\boldsymbol{a}_{0,1}}^{\substack{2\text{nd}\\ \text{time}}}\cdots\overbrace{\boldsymbol{a}_{0,M-1}}^{\substack{M\text{th}\\ \text{time}}}}_{\text{1st frequency}} | \underbrace{\boldsymbol{a}_{1,0}\boldsymbol{a}_{1,1}\cdots\boldsymbol{a}_{1,M-1}}_{\text{2nd frequency}} | \cdots | \underbrace{\boldsymbol{a}_{N-1,0}\boldsymbol{a}_{N-1,1}\cdots\boldsymbol{a}_{N-1,M-1}}_{N\text{th frequency}}]. \tag{8}$$

© The Institution of Engineering and Technology 2015

channel coefficient of the rth path [27], which we assume is zero-mean circular symmetric complex Gaussian. We also assume that channel coefficients related to different paths are uncorrelated. We consider, $N_{\text{cp}} \geq L$. Received vector of length $N_{\text{CP}} + NM + L - 1$ is given by,

$$\boldsymbol{y}_{\text{cp}} = \boldsymbol{h} \times \boldsymbol{x}_{\text{cp}} + \boldsymbol{v}_{\text{cp}}, \tag{10}$$

where ν_{cp} is the AWGN vector of length $MN + N_{\text{cp}} + L - 1$ with elemental variance σ_v^2. The first N_{cp} samples and last $L-1$ samples of $\boldsymbol{y}_{\text{cp}}$ are removed at the receiver, that is, $\boldsymbol{y} = [\boldsymbol{y}_{\text{cp}}(N_{\text{cp}} + 1{:}N_{\text{cp}} + MN)]$. Use of CP converts linear channel convolution to circular channel convolution when $N_{\text{cp}} \geq L$ [1]. The MN length received vector after removal of CP can be written as,

$$\boldsymbol{y} = \boldsymbol{HA}\tilde{\boldsymbol{d}} + \boldsymbol{v}, \tag{11}$$

where $\boldsymbol{H}$ is the circulant convolution matrix of size $MN \times MN$, which can be written as,

$$\boldsymbol{H} = \begin{bmatrix} h_1 & 0 & \cdots & 0 & h_L & \cdots & h_2 \\ h_2 & h_1 & \cdots & 0 & 0 & \cdots & h_3 \\ \vdots & & \ddots & & & & \\ h_L & h_{L-1} & \cdots & \cdots & \cdots & \cdots & 0 \\ 0 & h_L & \cdots & \cdots & \cdots & \cdots & 0 \\ \vdots & & \ddots & & & & \\ 0 & 0 & & h_L & \cdots & \cdots & h_1 \end{bmatrix}, \tag{12}$$

and ν is the WGN vector of length MN with elemental variance σ_v^2. Received vector $\boldsymbol{y}$ is distorted due to (i) self-interference as subcarriers are non-orthogonal [23] and (ii) ICI due to FSFC.

3 BER computation for MMSE receiver

3.1 MMSE receiver

To equalise the channel and GFDM induced self-interference, a joint MMSE equaliser [19] is considered here. Equalised data can be given as,

$$\begin{aligned} \hat{\boldsymbol{d}} &= \left[\boldsymbol{I}_{MN}\frac{\sigma_v^2}{\sigma_d^2} + (\boldsymbol{HA})^{\text{H}}(\boldsymbol{HA})\right]^{-1}(\boldsymbol{HA})^{\text{H}}\boldsymbol{y} \\ &= \boldsymbol{\mathcal{B}}\boldsymbol{d} + \boldsymbol{\mathcal{C}}\boldsymbol{v}, \end{aligned} \tag{13}$$

where $\boldsymbol{\mathcal{B}} = [\boldsymbol{I}_{MN}(\sigma_{v^2}/\sigma_{d^2}) + (\boldsymbol{HA})^{\text{H}}(\boldsymbol{HA})]^{-1}(\boldsymbol{HA})^{\text{H}}(\boldsymbol{HA})$ and $\boldsymbol{\mathcal{C}} = [\boldsymbol{I}_{MN}(\sigma_{v^2}/\sigma_{d^2}) + (\boldsymbol{HA})^{\text{H}}(\boldsymbol{HA})]^{-1}(\boldsymbol{HA})^{\text{H}}$. First term in the above equation holds desired plus interference values and second term holds the post-processing noise values.

3.2 SINR computation

Suppose we want to detect lth symbol. Estimated lth symbol can be given as,

$$\hat{d}_l = [\boldsymbol{\mathcal{B}}]_{l,l}d_l + \sum_{r=0, r\neq l}^{MN-1}[\boldsymbol{\mathcal{B}}]_{l,r}d_r + \sum_{r=0}^{MN-1}[\boldsymbol{\mathcal{C}}]_{l,r}\nu_r, \tag{14}$$

where first term is the desired term, second term is the interference term and third term is the post-processed noise term. Using the above equation, $E[|\hat{d}_l|^2] = \sigma_d^2[\boldsymbol{\mathcal{B}}]_{l,l}^2 + \sigma_d^2\sum_{r=0,r\neq l}^{MN-1}|[\boldsymbol{\mathcal{B}}]_{l,r}|^2 + \sigma_v^2\sum_{r=0}^{MN-1}|[\boldsymbol{\mathcal{C}}]_{l,r}|^2$, where the first term is the average signal power $P_{\text{Sig},l}$, the second term is the average interference power $P_{\text{Sig+Inr},l}$ and the third term is the average post-processing noise power $P_{\text{Npp},l}$. Using (13), $E[\hat{\boldsymbol{d}}\hat{\boldsymbol{d}}^{\text{H}}] = \sigma_d^2\boldsymbol{\mathcal{B}}\boldsymbol{\mathcal{B}}^{\text{H}} + \sigma_v^2\boldsymbol{\mathcal{C}}\boldsymbol{\mathcal{C}}^{\text{H}}$, where diagonal values of the first matrix term holds average signal plus interference power $P_{\text{Sig+Inr},l}$, diagonal values of the second matrix term holds average post-processing noise power, $\boldsymbol{\mathcal{B}}\boldsymbol{\mathcal{B}}^{\text{H}} = [[\boldsymbol{I}_{MN}(\sigma_{v^2}/\sigma_{d^2}) + (\boldsymbol{HA})^{\text{H}}(\boldsymbol{HA})]^{-1}(\boldsymbol{HA})^{\text{H}}(\boldsymbol{HA})]^2 = \boldsymbol{\mathcal{B}}^2$ and $\boldsymbol{\mathcal{C}}\boldsymbol{\mathcal{C}}^{\text{H}} = [\boldsymbol{I}_{MN}(\sigma_{v^2}/\sigma_{d^2}) + (\boldsymbol{HA})^{\text{H}}(\boldsymbol{HA})]^{-1}(\boldsymbol{HA})^{\text{H}}(\boldsymbol{HA})\ [\boldsymbol{I}_{MN}(\sigma_{v^2}/\sigma_{d^2}) + (\boldsymbol{HA})^{\text{H}}(\boldsymbol{HA})]^{-1}$. Using this, average signal power $P_{\text{Sig},l}$ and average interference power $P_{\text{Inr},l}$, average signal plus interference power $P_{\text{Sig+Inr},l}$ and post-processed noise power $P_{\text{Npp},l}$ for the lth symbol can be given as,

$$\begin{aligned} &P_{\text{Sig},l} = \sigma_{d^2}|[\boldsymbol{\mathcal{B}}]_{l,l}|^2,\ P_{\text{Sig+Inr},l} = \sigma_{d^2}|[\boldsymbol{\mathcal{B}}\boldsymbol{\mathcal{B}}^{\text{H}}]_{l,l}|, \\ &P_{\text{Inr},l} = P_{\text{Sig+Inr},l} - P_{\text{Sig},l} \text{ and } P_{\text{Npp},l} = \sigma_{v^2}|[\boldsymbol{\mathcal{C}}\boldsymbol{\mathcal{C}}^{\text{H}}]_{l,l}|. \end{aligned} \tag{15}$$

SINR for the lth symbol can be computed as,

$$\gamma_l = \frac{P_{\text{Sig},l}}{P_{\text{Inr},l} + P_{\text{Npp},l}} \tag{16}$$

Now we will compute SINR for FSFC and AWGN channel separately.

3.2.1 FSFC: Both $\boldsymbol{\mathcal{B}}$ and $\boldsymbol{\mathcal{C}}\boldsymbol{\mathcal{C}}^{\text{H}}$ involve $(\boldsymbol{HA})^{\text{H}}(\boldsymbol{HA})$. To compute (16) we explore the product. $(\boldsymbol{HA})^{\text{H}}\boldsymbol{HA}$ is a Hermitian matrix and hence it can be diagonalised as, $(\boldsymbol{HA})^{\text{H}}\boldsymbol{HA} = \boldsymbol{V}\boldsymbol{\Lambda}\boldsymbol{V}^{\text{H}}$, where, $\boldsymbol{V}$ is a unitary matrix which holds eigenvectors of $(\boldsymbol{HA})^{\text{H}}\boldsymbol{HA}$ in its columns and $\boldsymbol{\Lambda} = \text{diag}\{\lambda_0, \lambda_1, \ldots, \lambda_{MN-1}\}$ is a diagonal matrix which holds eigenvalues of $(\boldsymbol{HA})^{\text{H}}\boldsymbol{HA}$. We can write, $\boldsymbol{\mathcal{B}} = \boldsymbol{V}\tilde{\boldsymbol{\Lambda}}\boldsymbol{V}^{\text{H}}$, where $\tilde{\boldsymbol{\Lambda}} = \text{diag}\{\tilde{\lambda}_0, \tilde{\lambda}_1, \ldots, \tilde{\lambda}_{MN-1}\}$, $\tilde{\lambda}_s = \lambda_s/((\sigma_v^2/\sigma_d^2) + \lambda_s)$ and $\boldsymbol{\mathcal{C}}\boldsymbol{\mathcal{C}}^{\text{H}} = \boldsymbol{V}\tilde{\tilde{\boldsymbol{\Lambda}}}\boldsymbol{V}^{\text{H}}$, where $\tilde{\tilde{\boldsymbol{\Lambda}}} = \text{diag}\{\tilde{\tilde{\lambda}}_0, \tilde{\tilde{\lambda}}_1, \ldots, \tilde{\tilde{\lambda}}_{MN-1}\}$ and $\tilde{\tilde{\lambda}}_s = \lambda_s/((\sigma_v^2/\sigma_d^2) + \lambda_s)^2$. Putting values of $\boldsymbol{\mathcal{B}}$ and $\boldsymbol{\mathcal{C}}$ into (15), we can get,

$$\begin{aligned} &P_{\text{Sig},l} = \sigma_{d^2}|[\boldsymbol{V}\tilde{\boldsymbol{\Lambda}}\boldsymbol{V}^{\text{H}}]_{l,l}|^2,\ P_{\text{Inr},l} = \sigma_{d^2}|\sum_{r=0,r\neq l}^{MN-1}[\boldsymbol{V}\tilde{\boldsymbol{\Lambda}}\boldsymbol{V}^{\text{H}}]_{l,r}|^2 \text{ and} \\ &P_{\text{Npp},l} = \sigma_{v^2}|[\boldsymbol{V}\tilde{\tilde{\boldsymbol{\Lambda}}}\boldsymbol{V}^{\text{H}}]_{l,l}|^2. \end{aligned} \tag{17}$$

Through the reduction, complex expression involving matrix inverse as in (14), is brought to a simpler form (using eigenvalue decomposition of $(\boldsymbol{HA})^{\text{H}}\boldsymbol{HA}$), that is, instead of computing $\boldsymbol{\mathcal{B}}$ we can proceed directly with $\boldsymbol{HA}$.

3.2.2 AWGN: In case of AWGN, $\boldsymbol{H} = \boldsymbol{I}_{MN}$, hence we can write the following,

$$\begin{aligned} &\boldsymbol{\mathcal{B}} = \left[\frac{\sigma_v^2}{\sigma_d^2}\boldsymbol{I} + \boldsymbol{A}^{\text{H}}\boldsymbol{A}\right]^{-1}\boldsymbol{A}^{\text{H}}\boldsymbol{A},\ \boldsymbol{\mathcal{C}} = \left[\frac{\sigma_v^2}{\sigma_d^2}\boldsymbol{I} + \boldsymbol{A}^{\text{H}}\boldsymbol{A}\right]^{-1}\boldsymbol{A}^{\text{H}} \text{ and} \\ &\boldsymbol{\mathcal{C}}\boldsymbol{\mathcal{C}}^{\text{H}} = \left[\frac{\sigma_v^2}{\sigma_d^2}\boldsymbol{I} + \boldsymbol{A}^{\text{H}}\boldsymbol{A}\right]^{-1}\boldsymbol{A}^{\text{H}}\boldsymbol{A}\left[\frac{\sigma_v^2}{\sigma_d^2}\boldsymbol{I} + \boldsymbol{A}^{\text{H}}\boldsymbol{A}\right]^{-1}. \end{aligned} \tag{18}$$

It can be seen that $\boldsymbol{A}^{\text{H}}\boldsymbol{A}$ is a major component of the analysis. It is important to study the $\boldsymbol{A}^{\text{H}}\boldsymbol{A}$ before we proceed further. We will see the properties of $\boldsymbol{A}_N^{\text{H}}\boldsymbol{A}_N$ below.

$\boldsymbol{A}_N^{\text{H}}\boldsymbol{A}_N$Matrix, $\boldsymbol{A}_N$, can be decomposed as

$$\boldsymbol{A}_N = \begin{bmatrix}[\boldsymbol{\mathcal{G}}_0\boldsymbol{E}]_{MN\times N} & \cdots & [\boldsymbol{\mathcal{G}}_{M-1}\boldsymbol{E}]_{MN\times N}\end{bmatrix}_{MN\times MN}, \tag{19}$$

where $\boldsymbol{\mathcal{G}}_p$'s be a set of $MN \times MN$ matrices, where $p = 0, \ldots, M-1$. Suppose the first matrix in the set $\boldsymbol{\mathcal{G}}_0 = \text{diag}\{\boldsymbol{g}^{\text{T}}\}$, where $\boldsymbol{g} = [g(0)g(1)\cdots g(MN-1)]^{\text{T}}$. Any matrix in the set can be written as a circularly shifted version of $\boldsymbol{\mathcal{G}}_0$ along its diagonals, that is, pth matrix in the set can be written as $\boldsymbol{\mathcal{G}}_p = \text{diag}\{\text{circshift}[\boldsymbol{g}^{\text{T}}, -pN]\}$, where circshift represents right

© The Institution of Engineering and Technology 2015

circular shift operation. $\mathcal{G}_p$ can be described as

$$\mathcal{G}_p = \begin{bmatrix} g(-pN)_{MN} & & \\ & \ddots & \\ & & g(-pN+MN-1)_{MN} \end{bmatrix}_{MN\times MN} \tag{20}$$

and $\boldsymbol{E} = [\mathbb{W}_N \cdots M\text{times} \cdots \mathbb{W}_N]^{\mathrm{T}}$ is an $MN \times N$ matrix, where $\mathbb{W}_N$ is the $N \times N$ normalised inverse DFT matrix [28]. $[\boldsymbol{A}_N^{\mathrm{H}}\boldsymbol{A}_N]_{r,q} = \boldsymbol{E}^{\mathrm{H}}\mathcal{G}_r^{\mathrm{H}}\mathcal{G}_q\boldsymbol{E}$, where $r, q = 0, \ldots, M-1$ and $\boldsymbol{E}^{\mathrm{H}}\mathcal{G}_r^{\mathrm{H}}\mathcal{G}_q\boldsymbol{E}$ is the $N \times N$ matrix. $[\boldsymbol{A}_N^{\mathrm{H}}\boldsymbol{A}_N]_{r,q}$ can be written as

$$[\boldsymbol{A}_N^{\mathrm{H}}\boldsymbol{A}_N]_{r,q}(\alpha,\ \beta) = \begin{cases} \sum_{\kappa=0}^{MN-1} b_\kappa, & \alpha = \beta \\ \sum_{\kappa=0}^{MN-1} \omega^{(\beta-\alpha)\kappa} b_\kappa, & \text{otherwise} \end{cases}, \tag{21}$$

where $\omega = \mathrm{e}^{\mathrm{j}2\pi/N}$, $b_\kappa = g((-rN+\kappa)_{MN})g((-qN+\kappa)_{MN})$, $r, q = 0 \cdots M-1$ and $\alpha, \beta = 0 \cdots N-1$. Let, $s = 0 \cdots N-1$

$$\begin{aligned}[\boldsymbol{A}_N^{\mathrm{H}}\boldsymbol{A}_N]_{r,q}((\alpha-s)_N,\ (\beta-s)_N) &= \sum_{\kappa=0}^{MN-1} \omega^{(\beta-s-\alpha+s)\kappa} b_\kappa \\ &= [\boldsymbol{A}_N^{\mathrm{H}}\boldsymbol{A}_N]_{r,q}(\alpha,\ \beta)\end{aligned} \tag{22}$$

This proves that each block $[\boldsymbol{A}_N^{\mathrm{H}}\boldsymbol{A}_N]_{r,q}$ of $\boldsymbol{A}_N^{\mathrm{H}}\boldsymbol{A}_N$ is circulant. Let, $\varsigma = 0, \ldots, M-1$.

$$\begin{aligned}&[\boldsymbol{A}_N^{\mathrm{H}}\boldsymbol{A}_N]_{(r-\varsigma)_M,(q-\varsigma)_M}(\alpha,\ \beta) \\ &= \sum_{\kappa=0}^{MN-1} \omega^{(\beta-\alpha)\kappa} g((-rN+\varsigma N+\kappa)_{MN})g((-qN+\varsigma N+\kappa)_{MN}).\end{aligned} \tag{23}$$

As ω is periodic with N and $g(\beta)$ is periodic with MN, $[\boldsymbol{A}_N^{\mathrm{H}}\boldsymbol{A}_N]_{(r-\varsigma)_M,(q-\varsigma)_M}(\alpha,\ \beta) = [\boldsymbol{A}_N^{\mathrm{H}}\boldsymbol{A}_N]_{r,q}(\alpha,\ \beta)$; hence, $\boldsymbol{A}_N^{\mathrm{H}}\boldsymbol{A}_N$ is the block circulant matrix with circulant blocks (BCCBs) with blocks of size $N \times N$. In the same way, it can be proved that $\boldsymbol{A}_M^{\mathrm{H}}\boldsymbol{A}_M$ is also BCCB with blocks of size $M \times M$.

Using the properties of BCCB matrix one gets that [29] (i) inverse of BCCB matrix is a BCCB matrix, (ii) addition of a diagonal matrix with equal elements to a BCCB matrix is a BCCB matrix, (iii) multiplication of two BCCB matrix is a BCCB matrix. Hence, it can be easily proved that $\mathcal{B}$ and $\mathcal{C}\mathcal{C}^{\mathrm{H}}$ are also a BCCB in case of AWGN channel.

For any BCCB matrix [29] it can be shown that (i) diagonal elements are identical, (ii) all rows have equal power and (iii) all columns have equal power. Using this it can be then concluded that $P_{\mathrm{Sig},l} = P_{\mathrm{Sig}}$, $P_{\mathrm{Sig+Inr},l} = P_{\mathrm{Sig+Inr}}$, $P_{\mathrm{Inr},l} = P_{\mathrm{Inr}}$ and $P_{\mathrm{Npp},l} = P_{\mathrm{Npp}}$, $\forall l$. Therefore we can write, $[\mathcal{B}]_{l,l} = \mathrm{trace}\{\mathcal{B}\}/MN$, $[\mathcal{B}^2]_{l,l} = \mathrm{trace}\{\mathcal{B}^2\}/MN$ and $[\mathcal{C}\mathcal{C}^{\mathrm{H}}]_{l,l} = \mathrm{trace}\{\mathcal{C}\mathcal{C}^{\mathrm{H}}\}/MN$. Using this and (15), we can write

$$\begin{aligned}&P_{\mathrm{Sig}} = \frac{\sigma_d^2}{(MN)^2}\,\mathrm{trace}\{\mathcal{B}\}^2,\ P_{\mathrm{Sig+Inr}} = \frac{\sigma_d^2}{MN}\,\mathrm{trace}\{\mathcal{B}^2\}\ \text{and} \\ &P_{\mathrm{Npp}} = \frac{\sigma_v^2}{MN}\,\mathrm{trace}\{\mathcal{C}\mathcal{C}^{\mathrm{H}}\}.\end{aligned} \tag{24}$$

Now, using (18) in the above equation

$$\begin{aligned}P_{\mathrm{Sig}} &= \frac{\sigma_d^2}{(MN)^2}\left|\sum_{s=0}^{MN-1}\frac{\lambda_s}{\lambda_s + (\sigma_v^2/\sigma_d^2)}\right|^2, \\ P_{\mathrm{Sig+Inr}} &= \frac{\sigma_d^2}{MN}\sum_{s=0}^{MN-1}\left|\frac{\lambda_s}{\lambda_s + (\sigma_v^2/\sigma_d^2)}\right|^2 \text{ and} \\ P_{\mathrm{Npp}} &= \frac{\sigma_v^2}{MN}\sum_{s=0}^{MN-1}\frac{\lambda_s}{(\lambda_s + (\sigma_v^2/\sigma_d^2))^2}.\end{aligned} \tag{25}$$

SINR can be computed as

$$\gamma = \frac{P_{\mathrm{sig}}}{P_{\mathrm{Inr}+P_{\mathrm{Npp}}}}. \tag{26}$$

Hence, SINR can be computed using the eigenvalues of $\boldsymbol{A}^{\mathrm{H}}\boldsymbol{A}$. Through the above, because of the BCCB property, we can compute SINR easily than by using the direct form. Inversion of matrix $(\sigma_v^2/\sigma_d^2)\boldsymbol{I} + \boldsymbol{A}^{\mathrm{H}}\boldsymbol{A}$ needs complexity of $O(M^3N^3)$, whereas eigenvalue computation of $\boldsymbol{A}^{\mathrm{H}}\boldsymbol{A}$ needs complexity of $O(NM\log_2 N)$ [29]. Hence, SINR computation using the above method is much simpler than using direct matrix computation.

3.3 BER computation

3.3.1 FSFC channel: Fig. 3*a* shows cumulative distribution plot of noise plus interference value for 4-QAM modulated system for 3 and 9 dB E_b/N_0 values. Cumulative Distribution Function (CDF) plot for both cases is compared with Gaussian CDF with measured

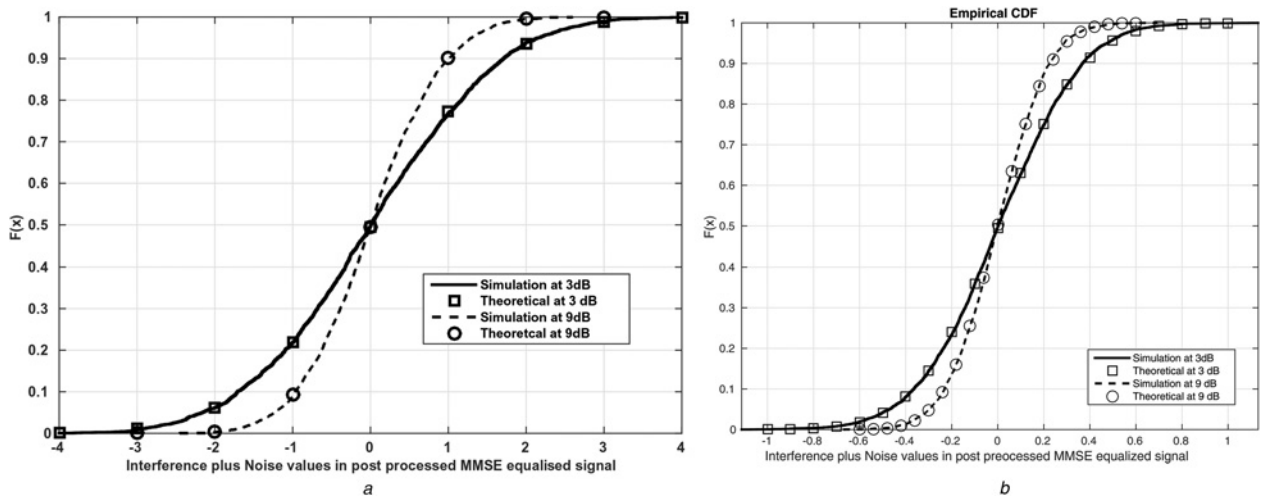

Fig. 3 *CDF plot of interference plus noise value in AWGN channel and FSFC for 4-QAM (pulse shaping filter is RRC with ROF = 0.5). (a) FSFC channel, (b) AWGN channel*

© The Institution of Engineering and Technology 2015

mean and variance values. It is clear from this figure that interference plus noise values closely follow Gaussian distribution.

Therefore, the BER for the lth QAM symbol with $\mathcal{M}$ modulation order can be computed as [30] by

$$P_{\mathrm{b}}(E|\gamma_l) \simeq 4\frac{\sqrt{\mathcal{M}}-1}{\sqrt{\mathcal{M}}\log_2(\mathcal{M})}\sum_{r=0}^{\sqrt{\mathcal{M}}/2-1}\left[Q\left\{(2r+1)\sqrt{\frac{3\gamma_l}{(\mathcal{M}-1)}}\right\}\right], \tag{27}$$

γ_l is the post-processing SINR for the lth symbol at the receiver given in (16). Average probability of error can be found as

$$P_b(E) = \frac{1}{MN}\times\sum_{l=0}^{MN-1}\int_0^{\infty}P_b(E|\gamma_l)f_{\gamma_l}(\gamma_l)\mathrm{d}\gamma_l, \tag{28}$$

where $f_{\gamma_l}(\gamma_l)$ is the probability density function of γ_l.

3.3.2 AWGN channel: Fig. 3*b* shows cumulative distribution plot of interference plus noise value (14) for 4-QAM modulated system for 3 and 9 dB E_{b}/N_0 values. As in case of FSFC, interference plus noise values closely follow Gaussian distribution. BER for QAM symbol with $\mathcal{M}$ modulation order can be computed as [30]

$$P_{\mathrm{b}}(E) \simeq 4\frac{\sqrt{\mathcal{M}}-1}{\sqrt{\mathcal{M}}\log_2(\mathcal{M})}\sum_{r=0}^{\sqrt{\mathcal{M}}/2-1}\left[Q\left\{(2r+1)\sqrt{\frac{3\gamma_l}{(\mathcal{M}-1)}}\right\}\right], \tag{29}$$

where γ is the post-processing SINR given in (26).

4 Precoded GFDM system

In this section, precoding schemes to enhance performance of GFDM are described. The first precoding scheme BIDFT is described in Section 4.1. The scheme is developed using special properties of $(\boldsymbol{HA})^{\mathrm{H}}\boldsymbol{HA}$ (detailed in Section 4.1.1) and $\boldsymbol{A}^{\mathrm{H}}\boldsymbol{A}$ (detailed in Section 3.2.1). For this precoding scheme there can be two kinds of receiver processing, namely, (i) joint processing: described in Section 4.1.1, which equalises channel and GFDM modulation matrix simultaneously, whereas (ii) two-stage processing: described in Section 4.1.2, first stage equalises for the channel and second stage equalises for GFDM modulation matrix. Two types of precoding matrices are defined for BIDFT precoding, namely, (i) BIDFT-M: where $\boldsymbol{A}$ is structured in blocks of $M\times M$, that is, $\boldsymbol{A}_M$ and (ii) BIDFT-N: where $\boldsymbol{A}$ is structured in blocks of $N\times N$, that is, $\boldsymbol{A}_N$. BIDFT-N precoded GFDM is processed using joint processing as well as two-stage processing, whereas BIDFT-M precoded GFDM is processed using two-stage processing only.

DFT-based precoding is described in Section 4.2. SVD-based precoding is described in Section 4.3. For each precoding scheme, precoder matrix $\boldsymbol{P}$, corresponding receivers and post-processing signal-to-noise ratio (SNR) are described in detail. Both BIDFT and DFT-based precoding does not require channel state information (CSI) at the transmitter to compute $\boldsymbol{P}$, whereas SVD-based precoding needs CSI at the transmitter to compute $\boldsymbol{P}$. Channel knowledge at the transmitter can be maintained via feedback from the receiver or through the reciprocity principle in a duplex system [31]. BER for precoded GFDM system is presented in Section 4.4. Computational complexities of GFDM and precoded GFDM system are given in Section 4.5.

4.1 BIDFT precoded GFDM

Received signal in (11) can be processed in two ways, (i) joint processing: channel and self-interference are equalised simultaneously and (ii) two-stage processing: channel and self-interference and equalised separately.

4.1.1 Joint processing: Suppose the received signal in (11) passed through an MF. Equalised vector which can be given as

$$\begin{aligned}\boldsymbol{y}^{\mathrm{MF}} &= (\boldsymbol{HAP})^{\mathrm{H}}\boldsymbol{y}\\ &= \boldsymbol{P}^{\mathrm{H}}(\boldsymbol{HA})^{\mathrm{H}}\boldsymbol{HAPd}+(\boldsymbol{HA})^{\mathrm{H}}\boldsymbol{v}.\end{aligned} \tag{30}$$

Since, $(\boldsymbol{HA})^{\mathrm{H}}\boldsymbol{HA}$ is multiplied to desired data vector in above equation. Now we will explore some properties of $(\boldsymbol{HA})^{\mathrm{H}}\boldsymbol{HA}$.

$(\boldsymbol{HA})^{\mathrm{H}}\boldsymbol{HA}$: Using, description of $\boldsymbol{A}_N$ given in Section 3.2.1, $(\boldsymbol{HA}_N)^{\mathrm{H}}\boldsymbol{HA}_N$ matrix can be given as

$$(\boldsymbol{HA}_N)^{\mathrm{H}}\boldsymbol{HA}_N = \begin{bmatrix}[\boldsymbol{L}_{0,0}]_{N\times N} & \cdots & [\boldsymbol{L}_{0,M-1}]_{N\times N}\\ \vdots & \ddots & \vdots\\ [\boldsymbol{L}_{M-1,0}]_{N\times N} & \cdots & [\boldsymbol{L}_{M-1,M-1}]_{N\times N}\end{bmatrix}_{MN\times MN}, \tag{31}$$

where $\boldsymbol{L}_{u,v}=\boldsymbol{E}^{\mathrm{H}}\boldsymbol{\mathcal{G}}_u^{\mathrm{H}}\boldsymbol{\Upsilon}\boldsymbol{\mathcal{G}}_v\boldsymbol{E}$ is an $N\times N$ submatrix or block, where $\boldsymbol{\Upsilon}=\boldsymbol{H}^{\mathrm{H}}\boldsymbol{H}$ is an $MN\times MN$ matrix and $u, v=0\cdots M-1$. Channel convolution matrix $\boldsymbol{H}$ is a circulant matrix and it can be shown that $\boldsymbol{\Upsilon}=\boldsymbol{H}^{\mathrm{H}}\boldsymbol{H}$ is also a circulant matrix using the properties of circulant matrices [28]. $(\boldsymbol{HA}_N)^{\mathrm{H}}\boldsymbol{HA}_N$ will be a block circulant matrix, iff, $\boldsymbol{L}_{(u+s)_M,(v+s)_M}=\boldsymbol{L}_{u,v}$, where $s=0\cdots M-1$. In the expression of $\boldsymbol{L}_{u,v}$, matrix $\boldsymbol{E}^{\mathrm{H}}$ and $\boldsymbol{E}$ are independent of block indices u, v. Therefore, it can be said that, $\boldsymbol{G}$ is a block circulant matrix, iff, $\boldsymbol{\Phi}_{(u+s)_M,(v+s)_M}=\boldsymbol{\Phi}_{u,v}$, where $\boldsymbol{\Phi}_{u,v}=\boldsymbol{\mathcal{G}}_u^{\mathrm{H}}\boldsymbol{\Upsilon}\boldsymbol{\mathcal{G}}_v$ is an $MN\times MN$ matrix. Let, $\boldsymbol{\Upsilon}=\{\upsilon_{r,q}\}_{MN\times MN}$ and using the definition of $\boldsymbol{\mathcal{G}}_p$, it can be shown that

$$\boldsymbol{\Phi}_{u,v}(r,\ q)=g_{(-uN+r)_{MN}}g_{(-vN+q)_{MN}}\upsilon_{r,q} \text{ and} \tag{32}$$

$$\boldsymbol{\Phi}_{(u+s)_M,(v+s)_M}(r,\ q)=g_{(-(u+s)N+r)_{MN}}g_{(-(v+s)N+q)_{MN}}\upsilon_{r,q}. \tag{33}$$

Substituting, $r'=r-sN$ and $q'=q-sN$, and since $\boldsymbol{\Upsilon}$ is a circulant matrix and hence $\upsilon_{(r'+sN,q'+sN)_{MN}}=\upsilon_{r',q'}$. Then, substituting r' and q' with r and q,

$$\begin{aligned}\boldsymbol{\Phi}_{(u+s)_M,(v+s)_M}(r,\ q) &= g_{(-uN+r)_{MN}}g_{(-vN+q)_{MN}}\upsilon_{r,q}\\ &= \boldsymbol{\Phi}_{(u)_M,(v)_M}(r,\ q)\end{aligned} \tag{34}$$

Hence $(\boldsymbol{HA}_N)^{\mathrm{H}}\boldsymbol{HA}_N$ is a block circulant matrix with blocks of size $N\times N$. (It may be noted here that $(\boldsymbol{HA}_M)^{\mathrm{H}}\boldsymbol{HA}_M$ will not be block circulant with blocks of size $M\times M$.). Since $(\boldsymbol{HA}_N)^{\mathrm{H}}\boldsymbol{HA}_N$ is block circulant matrix with blocks of size $N\times N$, it can be decomposed as given in [29, 32], as, $(\boldsymbol{HA}_N)^{\mathrm{H}}\boldsymbol{HA}_N=\boldsymbol{F}_{bN}\boldsymbol{D}_{bN}\boldsymbol{F}_{bN}^{\mathrm{H}}$, where $\boldsymbol{F}_{bN}=\begin{bmatrix}\boldsymbol{W}_N^0 & \boldsymbol{W}_N & \cdots & \boldsymbol{W}_N^{M-1}\end{bmatrix}_{MN\times MN}$, where $\boldsymbol{W}_N^i=\frac{\begin{bmatrix}\boldsymbol{I}_N & w_N^i\boldsymbol{I}_N & \cdots & w_N^{i(N-1)}\boldsymbol{I}_N\end{bmatrix}_{N\times MN}^{\mathrm{T}}}{\sqrt{N}}$, where $w_N=\mathrm{e}^{\mathrm{j}2\pi/N}$ and $\boldsymbol{D}_{bN}=\mathrm{diag}\{\boldsymbol{D}_{bN}^0\boldsymbol{D}_{bN}^1\cdots\boldsymbol{D}_{bN}^{M-1}\}$ is block diagonal matrix with blocks of size $N\times N$, where $\boldsymbol{D}_{bN}^r$ is the rth diagonal matrix of size $N\times N$.

Using this decomposition and taking $\boldsymbol{A}$ as $\boldsymbol{A}_N$, MF output in (30) can be written as

$$\boldsymbol{y}^{\mathrm{MF}}=\boldsymbol{P}^{\mathrm{H}}\boldsymbol{F}_{bN}\boldsymbol{D}_{bN}\boldsymbol{F}_{bN}^{\mathrm{H}}\boldsymbol{Pd}+(\boldsymbol{HA}_N)^{\mathrm{H}}\boldsymbol{v}. \tag{35}$$

BIDFT-N precoding: If we choose, $\boldsymbol{P}=\boldsymbol{F}_{\mathrm{b}N}$ (call it BIDFT-N

IET Commun., 2015, Vol. 9, Iss. 15, pp. 1829–1841
© The Institution of Engineering and Technology 2015

(BIDFTN) precoding), then

$$\begin{aligned} \boldsymbol{y}^{\mathrm{MF}} &= \boldsymbol{D}_{\mathrm{b}N}\boldsymbol{d} + (\boldsymbol{H}\boldsymbol{A}_N)^{\mathrm{H}}\boldsymbol{\nu} \\ &= \begin{bmatrix} \boldsymbol{D}_{\mathrm{b}N}^0 & & & \\ & \boldsymbol{D}_{\mathrm{b}N}^1 & & \\ & & \ddots & \\ & & & \boldsymbol{D}_{\mathrm{b}N}^{N-1} \end{bmatrix} \begin{bmatrix} \boldsymbol{d}_0^N \\ \boldsymbol{d}_1^N \\ \vdots \\ \boldsymbol{d}_{M-1}^N \end{bmatrix} + \bar{\boldsymbol{\nu}}, \end{aligned} \tag{36}$$

where $\bar{\boldsymbol{\nu}}$ is the MF processed noise vector. In the above equation, $\boldsymbol{D}_{bN}$ being block diagonal matrix, adds only $N-1$ interfering symbols instead $MN-1$ (in case of uncoded GFDM). This shows that precoding reduces the number of interfering symbols significantly. ZF equalisation is applied to reduce interference further. Multiplying $\boldsymbol{D}_{bN}^{-1}$ in the above equation we get

$$\hat{\boldsymbol{d}}_{\mathrm{BIDFT}}^{\mathrm{JP}} = \boldsymbol{d} + \boldsymbol{\nu}_{\mathrm{BIDFT}}^{\mathrm{JP}}, \tag{37}$$

where $\boldsymbol{\nu}_{\mathrm{BIDFT}}^{\mathrm{JP}} = \boldsymbol{D}_{bN}^{-1}(\boldsymbol{H}\boldsymbol{A}_N)^{\mathrm{H}}\boldsymbol{\nu}$ is the post-processing noise vector and superscript JP signifies that signal processing steps followed in this method are joint processing (channel and self-interference are equalised jointly). $\boldsymbol{D}_{bN}$ can be computed as

$$\boldsymbol{D}_{bN} = \boldsymbol{F}_{bN}^{\mathrm{H}}(\boldsymbol{H}\boldsymbol{A}_N)^{\mathrm{H}}\boldsymbol{H}\boldsymbol{A}_N\boldsymbol{F}_{bN}. \tag{38}$$

Post-processing SNR for the lth symbol can be obtained as

$$\gamma_{\mathrm{BIDFT},l}^{\mathrm{JP}} = \frac{\sigma_{d^2}}{E[\boldsymbol{\nu}_{\mathrm{BIDFT}}^{\mathrm{JP}}(\boldsymbol{\nu}_{\mathrm{BIDFT}}^{\mathrm{JP}})^{\mathrm{H}}]_{l,l}}, \tag{39}$$

where denominator in the above equation is post-processing noise power for the lth symbol.

4.1.2 Two-stage processing: In the above method, channel and GFDM were equalised together. In this method, we will first equalise channel distortions, and then GFDM induced self-interference. As explained in Section 1, $\boldsymbol{H}$ is a circulant matrix. Hence, $\boldsymbol{H}$ can be decomposed as

$$\boldsymbol{H} = \boldsymbol{W}_{NM}\boldsymbol{\Psi}\boldsymbol{W}_{NM}^{\mathrm{H}}, \tag{40}$$

where $\boldsymbol{W}_{NM}$ is the normalised IDFT matrix of size $MN \times MN$ and $\boldsymbol{\Psi} = \mathrm{diag}\{\upsilon_0, \upsilon_1, \ldots, \upsilon_{MN-1}\}$ is a diagonal matrix. Channel equalised vector can be obtained as

$$\boldsymbol{y}_{\mathrm{FDE}} = \boldsymbol{W}_{NM}^{\mathrm{H}}\boldsymbol{\Psi}^{-1}\boldsymbol{W}_{NM}\boldsymbol{y} = \boldsymbol{A}\boldsymbol{P}\boldsymbol{d} + \boldsymbol{W}_{NM}\boldsymbol{\Psi}^{-1}\boldsymbol{W}_{NM}^{\mathrm{H}}\boldsymbol{\nu}, \tag{41}$$

where first term is the transmitted signal which is free from channel distortions completely, second term is an enhanced noise and subscript FDE is acronym for frequency-domain equalisation (as above-described channel equalisation is FDE [1]). $\boldsymbol{\Psi}$ can be obtained as $\boldsymbol{\Psi} = \boldsymbol{W}_{NM}^{\mathrm{H}}\boldsymbol{H}\boldsymbol{W}_{NM}$ which equivalently obtained by taking NM point fast Fourier transform (FFT) of zero padded channel convolution vector $\boldsymbol{h}$ which is also the first column of $\boldsymbol{H}$ [1, 2].

Now passing channel equalised data $\boldsymbol{y}_{\mathrm{FDE}}$ to MF receiver, we can get

$$\begin{aligned} \boldsymbol{y}_{\mathrm{FDE-MF}} &= (\boldsymbol{A}\boldsymbol{P})^{\mathrm{H}}\boldsymbol{y}_{\mathrm{FDE}} \\ &= \boldsymbol{P}^{\mathrm{H}}\boldsymbol{A}^{\mathrm{H}}\boldsymbol{A}\boldsymbol{P}\boldsymbol{d} + (\boldsymbol{A}\boldsymbol{P})^{\mathrm{H}}\boldsymbol{W}_{NM}\boldsymbol{\Psi}^{-1}\boldsymbol{W}_{NM}^{\mathrm{H}}\boldsymbol{\nu}. \end{aligned} \tag{42}$$

It has been proved in Section 3.2.2 that $\boldsymbol{A}^{\mathrm{H}}\boldsymbol{A}$ is the BCCB matrix with blocks of size either $N \times N$ or $M \times M$, which depends on whether $\boldsymbol{A} = \boldsymbol{A}_N$ or $\boldsymbol{A} = \boldsymbol{A}_M$. Which are described next.

BIDFT-N precoding: When modulation matrix is defined as $\boldsymbol{A}_N$, $\boldsymbol{A}_N^{\mathrm{H}}\boldsymbol{A}_N$ can be decomposed as

$$\boldsymbol{A}_N^{\mathrm{H}}\boldsymbol{A}_N = \boldsymbol{F}_{bN}\tilde{\boldsymbol{D}}_{bN}\boldsymbol{F}_{bN}^{\mathrm{H}}, \tag{43}$$

where $\tilde{\boldsymbol{D}}_{bN} = \mathrm{diag}\{\boldsymbol{D}_{bN}^0, \boldsymbol{D}_{bN}^1, \ldots, \boldsymbol{D}_{bN}^{M-1}\}$ is the $MN \times MN$ block diagonal matrix where $\boldsymbol{D}_{bN}^r$ is the rth diagonal block of size $N \times N$. Choosing, $\boldsymbol{P} = \boldsymbol{F}_{\mathrm{b}N}$ (BIDFTN precoding) and using the above decomposition, MF output in (42) can be written as

$$\boldsymbol{y}_{\mathrm{FDE-MF}} = \tilde{\boldsymbol{D}}_{\mathrm{b}N}\boldsymbol{d} + (\boldsymbol{A}\boldsymbol{F}_{\mathrm{b}N})^{\mathrm{H}}\boldsymbol{W}_{NM}\boldsymbol{\Psi}^{-1}\boldsymbol{W}_{NM}^{\mathrm{H}}\boldsymbol{\nu}. \tag{44}$$

Now multiplying $\tilde{\boldsymbol{D}}_{bN}^{-1}$ in the above equation

$$\hat{\boldsymbol{d}}_{\mathrm{FDE-MF-ZF}}^N = \boldsymbol{d} + \boldsymbol{\nu}_{\mathrm{FDE-MF-ZF}}^N, \tag{45}$$

where $\boldsymbol{\nu}_{\mathrm{FDE-MF-ZF}}^N = \tilde{\boldsymbol{D}}_{bN}^{-1}(\boldsymbol{A}\boldsymbol{F}_{bN})^{\mathrm{H}}\boldsymbol{W}_{NM}\boldsymbol{\Psi}^{-1}\boldsymbol{W}_{NM}^{\mathrm{H}}\boldsymbol{\nu}$ is an enhanced noise vector. Since $\tilde{\boldsymbol{D}}_{bN}$ needs to be computed to obtain $\hat{\boldsymbol{d}}_{\mathrm{FDE-MF}_{ZF}}^N$, it can be computed as, $\tilde{\boldsymbol{D}}_{bN} = \boldsymbol{F}_{bN}\boldsymbol{A}^{\mathrm{H}}\boldsymbol{A}\boldsymbol{F}_{bN}^{\mathrm{H}}$. Post-processing SNR for the lth symbol can be obtained as

$$\gamma_{\mathrm{FDE-MF-ZF},l}^N = \frac{\sigma_{d^2}}{E[\boldsymbol{\nu}_{\mathrm{FDE-MF-ZF}}^N(\boldsymbol{\nu}_{\mathrm{FDE-MF-ZF}}^N)^{\mathrm{H}}]_{l,l}}, \tag{46}$$

where denominator in the above equation is an enhanced noise power for the lth symbol.

BIDFT-M precoding: Now, if modulation matrix is defined as $\boldsymbol{A}_M$, $\boldsymbol{A}_M^{\mathrm{H}}\boldsymbol{A}_M = \boldsymbol{F}_{bM}\boldsymbol{D}_{bM}\boldsymbol{F}_{bM}^{\mathrm{H}}$, where $\boldsymbol{F}_{bM} = [\boldsymbol{W}_M^0 \ \boldsymbol{W}_M \ \cdots \ \boldsymbol{W}_M^{N-1}]_{MN \times MN}$, where $\boldsymbol{W}_M^r = \frac{[\boldsymbol{I}_M \ w_M^r\boldsymbol{I}_M \ \cdots \ w_M^{r(M-1)}\boldsymbol{I}_M]_{M \times MN}^{\mathrm{T}}}{\sqrt{M}}$, where $w_M = \mathrm{e}^{\mathrm{j}2\pi/M}$ and $\boldsymbol{D}_{bM} = \mathrm{diag}\{\boldsymbol{D}_{bM}^0\boldsymbol{D}_{bM}^1 \cdots \boldsymbol{D}_{bM}^{N-1}\}$ is the block diagonal matrix with blocks of size $M \times M$, where $\boldsymbol{D}_{bM}^r$ is the rth diagonal matrix of size $M \times M$. Using this decomposition, choosing $\boldsymbol{P} = \boldsymbol{F}_{\mathrm{b}M}$ (BIDFT-M (BIDFTM) precoding) and following same signal processing steps as in case of $\boldsymbol{A}_N$, equalised data vector can be given as

$$\hat{\boldsymbol{d}}_{\mathrm{FDE-MF}_{ZF}}^M = \boldsymbol{d} + \boldsymbol{\nu}_{\mathrm{FDE-MF-ZF}}^M, \tag{47}$$

where $\boldsymbol{\nu}_{\mathrm{FDE-MF-ZF}}^M = \boldsymbol{D}_{bM}^{-1}(\boldsymbol{A}\boldsymbol{F}_{bM})^{\mathrm{H}}\boldsymbol{W}_{NM}\boldsymbol{\Psi}^{-1}\boldsymbol{W}_{NM}^{\mathrm{H}}\boldsymbol{\nu}$ is enhanced noise vector. Since $\boldsymbol{D}_{\mathrm{b}M}$ needs to be computed to obtain $\hat{\boldsymbol{d}}_{\mathrm{FDE-MF}_{ZF}}^M$, it can be computed as

$$\boldsymbol{D}_{bM} = \boldsymbol{F}_{bM}\boldsymbol{A}^{\mathrm{H}}\boldsymbol{A}\boldsymbol{F}_{bM}^{\mathrm{H}}. \tag{48}$$

Post-processing SNR for the lth symbol can be obtained as

$$\gamma_{\mathrm{FDE-MF-ZF},l}^M = \frac{\sigma_{d^2}}{E[\boldsymbol{\nu}_{\mathrm{FDE-MF-ZF}}^M(\boldsymbol{\nu}_{\mathrm{FDE-MF-ZF}}^M)^{\mathrm{H}}]_{l,l}}, \tag{49}$$

where denominator in above equation is enhanced noise power for the lth symbol.

In summary, BIDFT precoding can be understood by Fig. 4*a*.

4.2 DFT precoded GFDM

DFT precoding has been used in OFDM systems [1, 2]. It has been shown that DFT precoding reduces PAPR significantly and is one of the optimum precoding matrices to reduce PAPR in OFDM systems [33]. This motivates us to investigate DFT precoded GFDM for reducing PAPR in GFDM system. Suppose, Q is spreading factor of the system then DFT order/size can be computed as, $N_{\mathrm{DFT}} = N/Q$. We assume that Q divides N completely. Two subcarrier mapping schemes are considered in this paper [34]: (i) localised frequency division multiple access (LFDMA) and (ii) interleaved frequency division multiple access (IFDMA).

Precoding matrix $\boldsymbol{P}$ can be defined as $\boldsymbol{P} = \boldsymbol{P}_m\boldsymbol{P}_c$, where $\boldsymbol{P}_c$ is a block diagonal matrix with each block being a DFT spreading

© The Institution of Engineering and Technology 2015

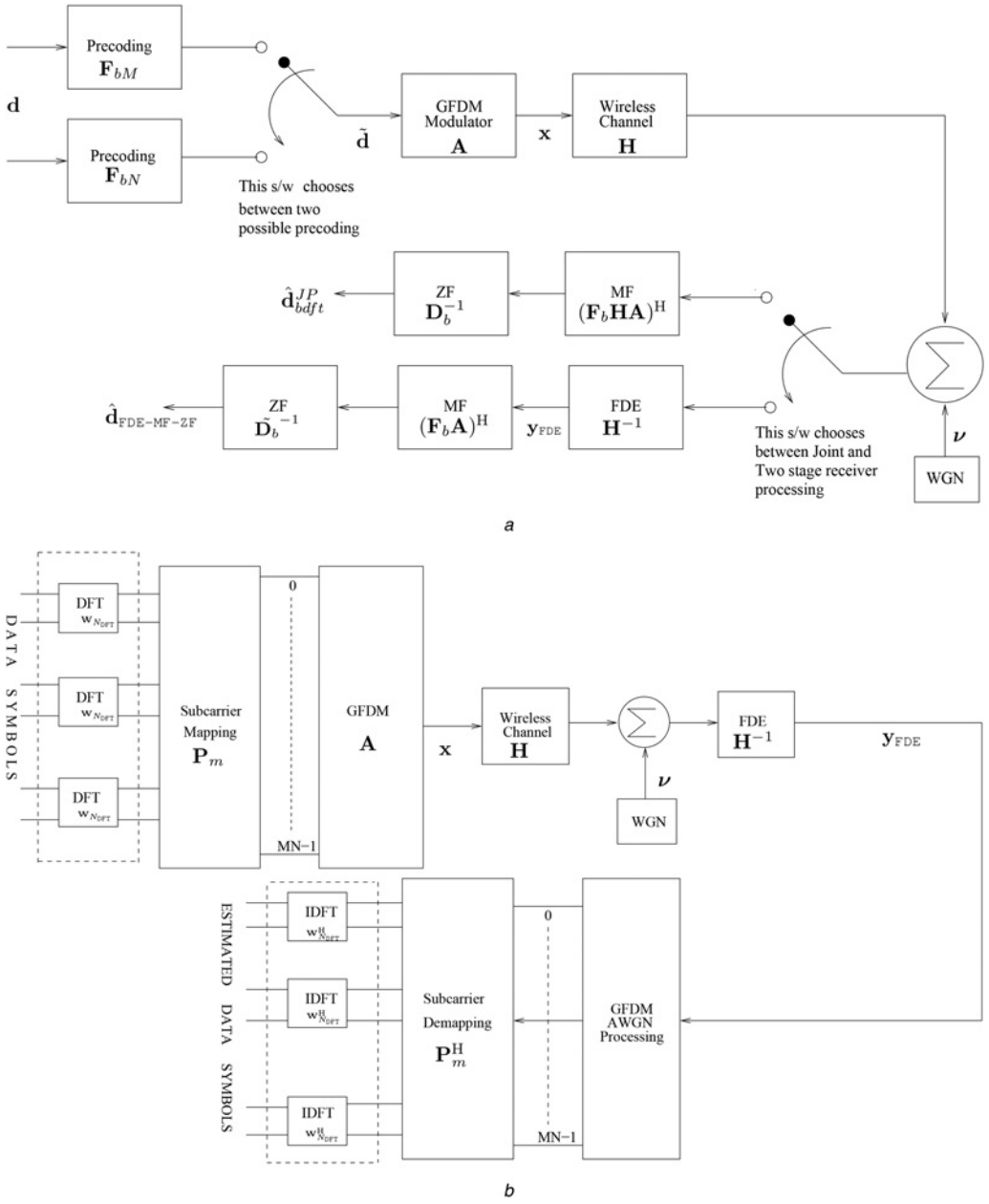

Fig. 4 *Block diagram of BIDFT and DFT precoded GFDM system. (a) BIDFT Precoded GFDM, (b) DFT Precoded GFDM*

matrix and $\boldsymbol{P}_m$ is a permutation matrix which implements subcarrier mapping, that is, LFDMA or IFDMA. The precoding spreading matrix $\boldsymbol{P}_c$ can be written as

$$\boldsymbol{P}_c = \begin{bmatrix} \boldsymbol{W}_{N_{\mathrm{DFT}}} & & & \\ & \boldsymbol{W}_{N_{\mathrm{DFT}}} & & \\ & & \ddots & \\ & & & \boldsymbol{W}_{N_{\mathrm{DFT}}} \end{bmatrix}, \tag{50}$$

where $\boldsymbol{W}_{N_{\mathrm{DFT}}}$ is the normalised DFT matrix of size $N_{\mathrm{DFT}} \times N_{\mathrm{DFT}}$. Permutation matrix $\boldsymbol{P}_m$ for LFDMA is an identity matrix. DFT precoded GFDM system can be understood from Fig. 4*b*. Precoded data vector is GFDM modulated using the modulation matrix $\boldsymbol{A}$. Received signal can be equalised using conventional linear [19, 23] or non-linear [24] equaliser. We will present here ZF receiver for DFT precoded GFDM. ZF equalised precoded data vector can be obtained as

$$\hat{\tilde{\boldsymbol{d}}}_{\mathrm{ZF}} = (\boldsymbol{HA})^{-1}\boldsymbol{y} = \tilde{\boldsymbol{d}} + (\boldsymbol{HA})^{-1}\boldsymbol{\nu}. \tag{51}$$

Equalised data vector $\hat{\boldsymbol{d}}_{\mathrm{DFT-spread}}$ can be obtained as

$$\begin{aligned} \hat{\boldsymbol{d}}_{\mathrm{DFT-spread}} &= \boldsymbol{P}^{\mathrm{H}}\hat{\tilde{\boldsymbol{d}}}_{\mathrm{ZF}} = \underbrace{\boldsymbol{P}_c^{\mathrm{H}}}_{\text{de-spreading}} \times \underbrace{\boldsymbol{P}_m^{\mathrm{H}}}_{\text{subcarrier de-mapping}} \times \hat{\tilde{\boldsymbol{d}}}_{\mathrm{ZF}} \\ &= \boldsymbol{d} + \boldsymbol{\nu}_{\mathrm{DFT-ZF}}, \end{aligned} \tag{52}$$

where $\nu_{\mathrm{DFT\text{-}ZF}} = \boldsymbol{P}^{\mathrm{H}}(\boldsymbol{HA})^{-1}\nu$ is the post-processing noise vector. Post-processing SNR for the lth symbol can be obtained as

$$\gamma_{\mathrm{DFT-ZF},l}^{N} = \frac{\sigma_{d^2}}{E[\boldsymbol{\nu}_{\mathrm{DFT-ZF}}^{N}(\boldsymbol{\nu}_{\mathrm{DFT-ZF}}^{N})^{\mathrm{H}}]_{l,l}}, \tag{53}$$

where denominator in above equation is enhanced noise power for the lth symbol.

IET Commun., 2015, Vol. 9, Iss. 15, pp. 1829–1841
© The Institution of Engineering and Technology 2015

4.3 SVD precoded GFDM

The product of the channel matrix and the modulation matrix ($\boldsymbol{HA}$) can be decomposed as

$$\boldsymbol{HA} = \boldsymbol{USV}^{\mathrm{H}}, \tag{54}$$

where $\boldsymbol{U}$ and $\boldsymbol{V}$ are unitary matrixes and $\boldsymbol{S}$ is the diagonal singular-value matrix, that is, $\boldsymbol{S} = \mathrm{diag}\{s_0, \backslash s_1, \ldots, s_r, \ldots, s_{MN-1}\}$, where s_r is the rth singular value. Then, $\boldsymbol{y}$ in (11), can be written as

$$\boldsymbol{y} = \boldsymbol{USV}^{\mathrm{H}}\boldsymbol{Pd} + \boldsymbol{v}. \tag{55}$$

At transmitter, by choosing $\boldsymbol{P} = \boldsymbol{V}$ (assuming ideal feedback channel) and multiplying both sides with $\boldsymbol{U}^{\mathrm{H}}$, the estimated symbol vector can be written as

$$\hat{\boldsymbol{d}}^{\mathrm{svd}} = \boldsymbol{Sd} + \boldsymbol{U}^{\mathrm{H}}\boldsymbol{v}. \tag{56}$$

The estimated lth symbol is then given by

$$\hat{d}_l^{\mathrm{svd}} = s_l d_l + \sum_{q=0}^{MN-1} [\boldsymbol{U}^{\mathrm{H}}]_{l,q}\nu(q). \tag{57}$$

From the above, it can be seen that by using SVD-based precoding, interference is completely removed by orthogonalisation of $\boldsymbol{HA}$ without the need for matrix inversion, which is required in ZF and MMSE receiver. SINR for the lth symbol, can be computed as

$$\gamma_l^{\mathrm{SVD}} = \frac{\sigma_d^2}{\sigma_v^2}|s_l|^2. \tag{58}$$

4.4 BER performance of precoding techniques

Expression for estimated data symbols, given in (37), (45), (47), (52) and (57), are summations of desired data symbols and enhanced noise vector. The enhanced noise vector is weighted sum of complex Gaussian random variable for a given channel realisation. Hence, enhanced noise is also complex Gaussian random vector for a given channel realisation. BER for QAM symbol with modulation order $\mathcal{M}$ over FSFC can be obtained as

$$P_b(E|\gamma_l) \simeq 4\frac{\sqrt{\mathcal{M}}-1}{\sqrt{\mathcal{M}}\log_2(\mathcal{M})}\sum_{r=0}^{\sqrt{\mathcal{M}}/2-1}\left[Q\left\{(2r+1)\sqrt{\frac{3\gamma_l}{(\mathcal{M}-1)}}\right\}\right], \tag{59}$$

where γ_l is the post-processing SNR computed in (39), (46), (49), (53) and (58). Average probability of error can be found as

$$P_b(E) = \frac{1}{MN}\times\sum_{l=0}^{MN-1}\int_0^{\infty} P_b(E|\gamma_l)f_{\gamma_l}(\gamma_l)\mathrm{d}\gamma_l, \tag{60}$$

where $f_{\gamma_l}(\gamma_l)$ is the probability distribution function of SINR for the lth symbol.

4.5 Computational complexity

Precoding schemes for GFDM are proposed in previous sections. It is utmost important to compute and compare the complexity of these systems as it is directly proportional to the cost of the system. Out of different mathematical operations, number of complex multiplication is a significant contributor to computational complexity [35]. Computation complexity is computed in terms of number of complex multiplication required to implement transmitter and receiver of precoded and uncoded GFDM systems. It has been assumed that modulation matrix $\boldsymbol{A}$ is known at the receiver, hence any matrix that is derived from $\boldsymbol{A}$ is also known to receiver, such as $\boldsymbol{A}^{\mathrm{H}}$, $\boldsymbol{A}^{-1}$ etc. All known receivers for uncoded GFDM are considered for complexity computation of uncoded GFDM and DFT precoded GFDM. Minimum number of complex multiplication required to perform various matrix and vector operations is computed. Complexity of SVD precoded GFDM receiver is computed for two cases, namely, (i) SVD of channel is (useful when channel is static for multiple transmit instances) and (ii) SVD of channel is unknown. Complexity computation can be found following Table 1.

5 Results

In this section, the results related to works described in earlier sections are presented. Analytical evaluation of BER of MMSE receiver with GFDM is given in Section 5.1. BER evaluation of precoded GFDM system is provided in Section 5.2. Complexities of different transmitters and receivers of GFDM and precoded GFDM are given in Section 5.3. Finally, PAPR of proposed precoding schemes is compared with GFDM and OFDM in Section 5.4. GFDM system with parameters given in Table 2 is considered here. It is assumed that the subcarrier bandwidth is larger than the coherence bandwidth of the channel for FSFC. SNR loss due to CP is also considered for FSFC.

5.1 BER evaluation of GFDM with MMSE receiver

BER against E_{b}/N_o for 16-QAM in AWGN and FSFC for MMSE receiver is presented in Fig. 5. Legends 'GFDM without self-interference' are obtained by using $\gamma_l = \sigma_d^2/\sigma_v^2$ in (28) for flat fading and in (29) for AWGN channel. This is a reference BER result for GFDM with zero self-interference and 16-QAM modulation in flat fading (28) and AWGN (29). The legends marked 'Analytical' are obtained by first computing γ_l using (16) for FSFC and using (26) for AWGN and then using this γ_l in (28) and (29) to obtain average BER for FSFC and AWGN, respectively. The legends marked 'Simu' are obtained using Monte Carlo simulations using parameters given in Table 2. It is seen that BER from simulation matches quite well with the analytical for both FSFC and AWGN. The gap between GFDM curve (analytical and simulation) and GFDM with no self-interference curve is due to self-interference encountered in GFDM [21]. From the above discussion, it can be concluded that the expressions developed in this paper are useful in estimating the theoretical BER for MMSE-based GFDM receiver in FSFC and AWGN channels.

5.2 BER evaluation of precoded techniques

BER of precoded GFDM system is evaluated via Monte Carlo simulations. Simulation parameters are given in Table 2. One thousand channel realisations are used to obtain the BER results. The legends GFDM–ZF, GFDM–MMSE and GFDM–D-SIC are used to represent the performance of the corresponding receivers for GFDM. The legends SVD precoded (SVD-Prec), BIDFTN, BIDFTM, BIDFT-JP, LFDMA-ZF and IFDMA-ZF are used to indicate the result of SVD-based precoding, BIDFTN precoding with two-stage processing, BIDFTM with two-stage processing, BIDFTN with joint processing, DFT precoding with IFDMA and DFT precoding with LFDMA, respectively. Legend OFDM-CP is used to indicate theoretical BER performance of OFDM-CP. Fig. 6 shows BER against E_{b}/N_o for ROF = 0.1 in AWGN channel and FSFC. The following observations can be made.

Under AWGN, all schemes have similar performance. It may be noted that in AWGN there is no SNR loss as CP is not required. The performance of GFDM is only slightly worst than OFDM. In the case of FSFC, it is seen that SVD, BIDFT-N-based precoding has performance similar to OFDM, as ICI is low because of small ROF. The better performance of DFT and BIDFT-M precoded

© The Institution of Engineering and Technology 2015

Table 1 Number of complex multiplication of different techniques in GFDM

Technique	Operations	Number of complex multiplications
GFDM Tx	one vector matrix multiplication for $\boldsymbol{y} = \boldsymbol{Ad}$	$(MN)^2$
GFDM Rx ZF–MF	(1) frequency-domain (ZF) • one FFT operation for $\boldsymbol{y}' = \boldsymbol{Wy}$ • one diagonal complex valued matrix inversion and one diagonal matrix and vector multiplication for $\boldsymbol{y}'' = \boldsymbol{\Lambda}^{-1}\boldsymbol{y}'$ • one FFT operation for $\boldsymbol{y}_{\text{FDE}} = \boldsymbol{Wy}''$ (2) MF for AWGN: one matrix vector multiplication for $\hat{\boldsymbol{d}}_{\text{ZF}} = \boldsymbol{A}^{\text{H}}\boldsymbol{y}_{\text{FDE}}$	$\frac{3MN}{2}\log_2(MN) + 2MN + (MN)^2$
GFDM Rx ZF–ZF	(1) frequency-domain (ZF): same operations as in ZF–MF (2) ZF for AWGN: one matrix vector multiplication for $\hat{\boldsymbol{d}}_{\text{MF}} = \boldsymbol{A}^{-1}\boldsymbol{y}_{\text{FDE}}$. Considering $\boldsymbol{A}^{-1}$ to be known and precomputed at the receiver	$\frac{3MN}{2}\log_2(MN) + 2MN + (MN)^2$
GFDM Rx ZF–MMSE	(1) frequency-domain (ZF): same operations as in ZF–MF (2) MMSE for AWGN • MN complex value addition for computing $\boldsymbol{C} = \frac{\boldsymbol{I}}{\gamma} + \boldsymbol{A}^{\text{H}}\boldsymbol{A}$ • one matrix inversion for computing $\boldsymbol{C}^{-1}$ • one matrix vector multiplication for $\boldsymbol{y}_{\text{temp}} = \boldsymbol{A}^{\text{H}}\boldsymbol{y}$ • one matrix vector multiplication for $\hat{\boldsymbol{d}}_{\text{MMSE}} = \boldsymbol{C}^{-1}\boldsymbol{y}_{\text{temp}}$	$\frac{3MN}{2}\log_2(MN) + \frac{(MN)^3}{3} + 2(MN)^2 + \frac{2MN}{3}$
GFDM Rx ZF–SIC	(1) frequency-domain (ZF): same operations as in ZF–MF (2) D-SIC for AWGN • MF operation to compute $\boldsymbol{y}_{\text{MF}}$ and $MN(\sqrt{\text{modorder}} - 1)$ comparators for detection of MF $\hat{\boldsymbol{d}}_{\text{detect}}$ • $2M$ complex multiplication and $2M$–1 complex addition are needed for each subcarrier and iteration index to compute $\boldsymbol{y}_k = \boldsymbol{Ad}_k$ where k is subcarrier index • MN complex subtraction is needed for each subcarrier and iteration index to compute $\boldsymbol{y}_{\text{interfree},k} = \boldsymbol{y}_{\text{MF}} - \boldsymbol{y}_k$	$\frac{3MN}{2}\log_2(MN) + 2MN + 2(MN)^2 J$
SVD-Prec GFDM Tx	two vector matrix multiplication for computing $\boldsymbol{AVd}$	$2(MN)^2$
SVD-Prec GFDM Rx (known SVD)	one vector matrix multiplication for computing $\boldsymbol{U}^{\text{H}}\boldsymbol{y}$	$(MN)^2$
SVD-Prec GFDM Rx (unknown SVD)	(1) SVD computation (2) one vector matrix multiplication for computing $\boldsymbol{U}^{\text{H}}\boldsymbol{y}$	$(MN)^2 + 26(MN)^3$
BIDFT precoded GFDM Tx	one vector matrix multiplication for computing $\boldsymbol{AF}_{\text{b}}\boldsymbol{d}$ as $\boldsymbol{AF}_{\text{b}}$ can be precomputed at transmitter	$(MN)^2$
BIDFT precoded GFDM Rx (joint processing)	(1) one vector matrix multiplication to compute $\boldsymbol{HAF}_{\text{b}}$ (2) computation of block diagonal matrix $\boldsymbol{D}_{\text{b}}$ (3) inversion $\boldsymbol{D}_{\text{b}}^{-1}$ which can be computed by inverting $\boldsymbol{M}$ square matrices of order N	$(MN)^2\log_2(N) + 2(MN)^2 + MN^2$
BIDFT precoded GFDM Rx (ZF–ZF)	(1) frequency-domain equalisation: same as in ZF–MF (2) AWGN processing: • one vector matrix multiplication for computing $\boldsymbol{y}_{\text{MF}} = (\boldsymbol{AF}_{\text{b}})^{\text{H}}\boldsymbol{y}$. • computation of block diagonal matrix $\boldsymbol{D}_{\text{b}}^{-1}$ • N times square matrix inversion of order M and block diagonal matrix and vector multiplication to compute $\hat{\boldsymbol{d}}_{\text{BIDFT}} = \boldsymbol{D}_{\text{b}}^{-1}\boldsymbol{y}_{\text{MF}}$	$\frac{3MN}{2}\log_2(MN) + 2MN + NM^2 + (MN)^2 + \underbrace{NM^2}_{\text{BIDFT}M}$ or $\underbrace{MN^2}_{\text{BIDFT}N}$
DFT precoded GFDM Tx (additional over GFDM Tx)	(1) additionally, MQ times N_{DFT} point FFT and subcarrier mapping (2) same operation as in GFDM Tx	$\frac{MN}{2}\log_2 N_{\text{DFT}}$
DFT precoded GFDM Rx (additional over GFDM Rx)	(1) same operation as in GFDM Rx (2) additionally, MQ times N_{DFT} point FFT and subcarrier mapping (3) same operation as in GFDM Tx	$\frac{MN}{2}\log_2 N_{\text{DFT}}$

GFDM over OFDM can be attributed to frequency diversity gain, which can be understood from Fig. 7.

In this figure, it can be seen that one symbol in BIDFT-M has larger frequency spread compared with IFDMA which is larger than LFDMA. Accordingly, BIDFTM precoded GFDM is performing better than IFDMA precoded GFDM which is performing better than LFDMA precoded GFDM.

Next we look at Fig. 8 which shows similar performance analysis for ROF 0.9, which indicates higher ICI. In case of AWGN, degradation can be observed as compared with Fig. 6. We see a similar degradation for all precoding schemes in FSFC. This is expected for ROF 0.9 as significant overlapping of pulses in frequency.

It is clear that the performance of precoding schemes is sensitive to ROF. In this paper, we have only considered RRC pulse shape. It is shown in [19, 20] that performance of uncoded GFDM is sensitive to pulse shape choice. Proposed precoded GFDM system will also be sensitive to pulse shape choice as the enhanced noise expressions in

IET Commun., 2015, Vol. 9, Iss. 15, pp. 1829–1841
© The Institution of Engineering and Technology 2015

Table 2 Simulation parameters of GFDM receivers

Number of subcarriers N	128
Number of timeslots M	5
Mapping	16-QAM
Pulse shape	RRC with ROF = 0.1 or 0.5 or 0.9
CP length N_{CP}	16
Channel	AWGN and FSFC
Channel length N_{ch}	16
Power delay profile	$[10^{-\alpha/5}]^T$, where $\alpha = 0, 1, \ldots, N_{ch} - 1$
Subcarrier bandwidth	3.9 kHz
RMS delay spread	4.3 μs
Coherence bandwidth	4.7 kHz

(36), (43), (46), (51) and (56) are functions of modulation matrix $\boldsymbol{A}$ which is a function of pulse shape as given in (7).

It can be concluded that precoding schemes are giving good performance over FSFC. BIDFTM precoded GFDM performs best among all precoding schemes.

5.3 Complexity computation

Table 3 compares the complexity of different transmitters and Table 4 compares the complexity of different receivers for two different application scenarios given in [19]. Table 5 shows values of N and M considered for different application scenarios. Complexity is computed in terms of number of complex multiplications. Complexities of precoded GFDM systems and uncoded GFDM systems are compared with OFDM system. Spreading factor, $Q = 4$, is considered for DFT precoded GFDM. GFDM receiver processing for DFT precoded GFDM is considered to be GFDM–ZF. Number of iterations for D-SIC receiver is considered to be 4 [24].

It is observed that the complexity of uncoded GFDM transmitter is about 100 times higher than OFDM transmitter in case of TI and, about 50 times greater than OFDM transmitter in case of wireless RAN (WRAN). BIDFT precoded and DFT precoded GFDM transmitters have the same order of complexity as uncoded GFDM transmitter. Complexity of SVD-Prec GFDM is around two times higher than uncoded GFDM transmitter. Therefore, it can be concluded that there is no significant increase in complexity for BIDFT and DFT precoded transmitters when compared with uncoded GFDM transmitter. However, for SVD-Prec transmitter complexity is doubled, which is also not a significant increment.

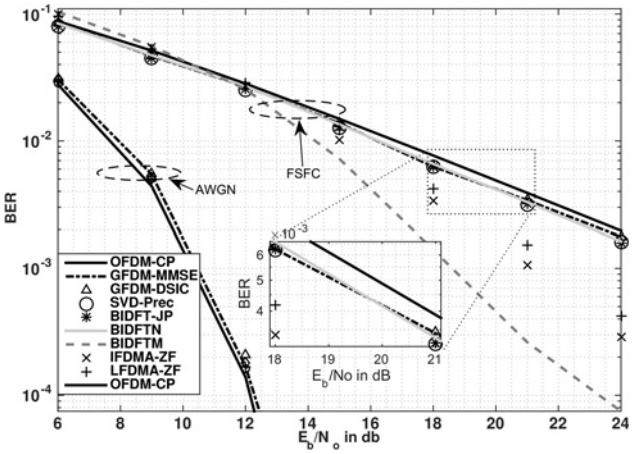

Fig. 6 *BER against E_b/N_o for Precoded GFDM Receiver over Frequency Selective and AWGN Channel using 16-QAM with $N = 128$, $M = 5$ and ROF = 0.1 (RRC)*

GFDM–ZF receiver complexity is much higher than OFDM receiver for instance 50 times in TI scenario. SVD-Prec GFDM receiver when SVD is known, two-stage BIDFT precoded receiver and DFT precoded receiver have around same complexities as GFDM–ZF receiver. GFDM–MMSE receiver has very high complexity, for example, 2000 times higher than GFDM–ZF in TI scenario. BIDFT precoded receiver complexity, when SVD of channel is not known, is even higher, for instance; it is 100 times higher than the complexity of GFDM–MMSE. It is also important to note that GFDM–D-SIC has higher complexity than GFDM–ZF, DFT precoded GFDM and two-stage BIDFT precoded GFDM.

5.4 PAPR of precoding techniques

The impact of precoding on PAPR is presented in Fig. 9. Complementary cumulative distribution function of PAPR is computed using Monte Carlo simulation. About 10^5 transmitted blocks were generated, where each block has two precoded GFDM symbols. For each precoded GFDM symbol: $N = 128$, $M = 5$ and ROF for RRC pulse shaping filter = 0.5. For OFDM, $N = 128$.

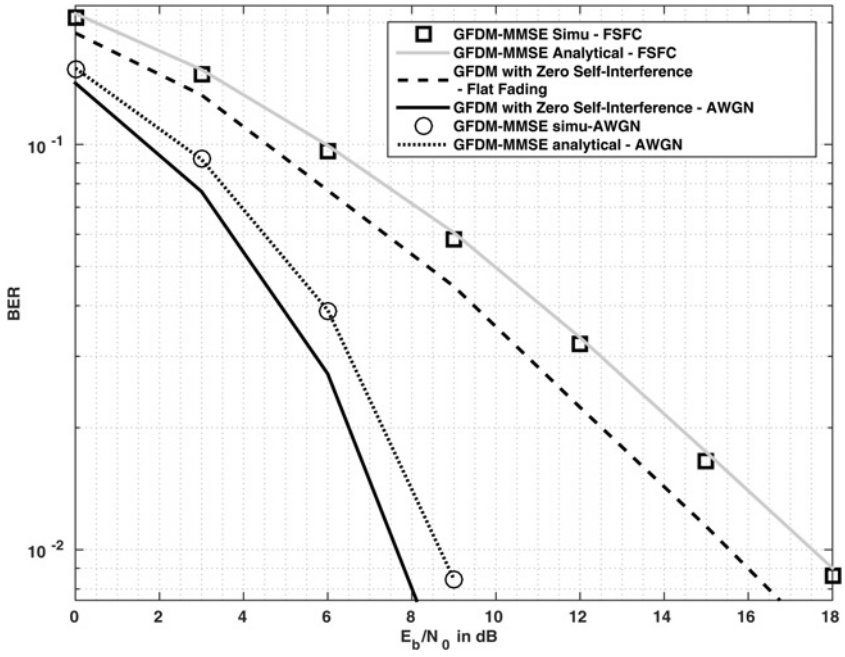

Fig. 5 *BER against E_b/N_o for MMSE GFDM receiver over AWGN and frequency selective channel for 16-QAM (RRC pulse shaping filter is used with ROF = 0.5)*

© The Institution of Engineering and Technology 2015

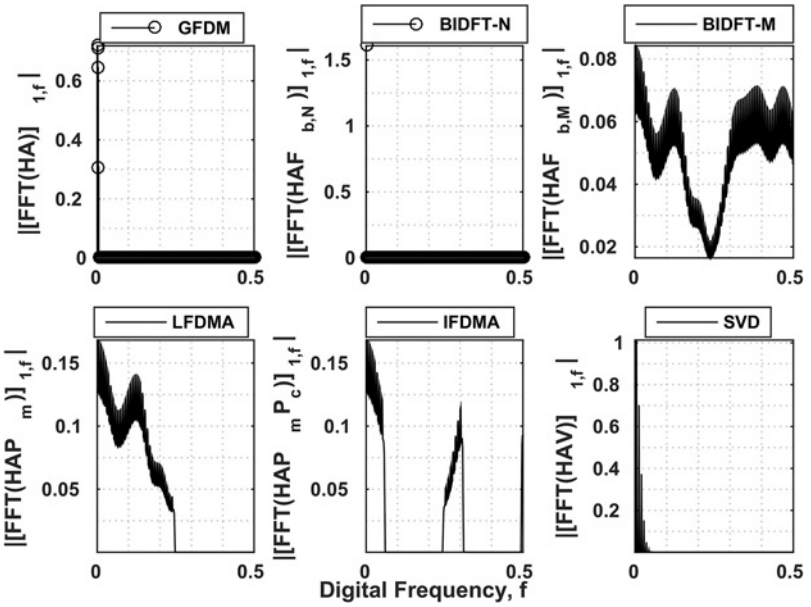

Fig. 7 *Frequency spread of one symbol for different transmission schemes*

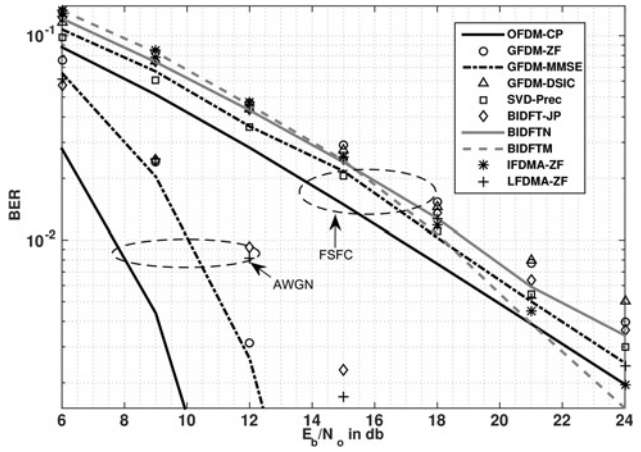

Fig. 8 *BER against E_b/N_o for precoded GFDM receiver over frequency selective and AWGN channel using 16-QAM with N = 128, M = 5 and ROF = 0.9 (RRC)*

Table 3 Number of complex multiplications for different transmitters

CASE	OFDM	Uncoded GFDM	SVD-Prec GFDM	BIDFT precoded GFDM	DFT precoded GFDM
TI	4.4×10^3	4.09×10^5	8.19×10^5	4.09×10^5	4.12×10^5
WRAN	8.1×10^3	4.1×10^5	8.25×10^5	4.12×10^5	4.13×10^5

Randomly generated data symbols are considered to be quadrature phase shift keying modulated.

As expected, GFDM has worst performance than OFDM. Precoding has a positive effect on GFDM. We compare the PAPR value that is exceeded with probability <0.1% (Pr{PAPR > PAPRo = 10^{-3}}). SVD-Prec GFDM and BIDFT*N* precoded GFDM reduces the PAPR by 0.3 dB but it is still higher than OFDM. DFT precoded GFDM with LFDMA subcarrier mapping reduces PAPR by 3.4 dB and is lower than OFDM. DFT precoded GFDM with IFDMA subcarrier mapping and BIDFT*M* precoded GFDM reduces PAPR by 9 dB.

6 Conclusion

GFDM, a possible waveform for 5G with flexibility to access time–frequency radio resources, is investigated in this paper. Two properties of GFDM system are proved (i) product of modulation matrix with its Hermitian is a BCCBs and (ii) product of circulant convolution channel matrix with the modulation matrix when multiplied with its Hermitian is block circulant matrix. An expression of SINR for MMSE receiver for GFDM is developed using matrix representation for the signal model. The SINR expression is determined in terms of eigenvalues of the product of modulation matrix with its Hermitian matrix for AWGN channel and in terms of eigenvalues and eigenvectors of product of circulant convolution channel matrix with the modulation matrix when multiplied with its Hermitian for FSFC. It is also shown that the addition of interference and noise values are Gaussian distributed. Using this BER is found. It is found that the BER obtained from simulation and that from the expression developed here match quite well in AWGN channel as well as in FSFC.

Three new precoding techniques which improve performance of GFDM system are proposed. The SVD-based precoding for GFDM removes interference by orthogonalising the received symbols. It does not require matrix inversion yet its performance is quite close to that of GFDM–MMSE result. The complexity of the receiver for such precoding is quite high when compared with GFDM–ZF receiver when SVD of channel is not known. However, when SVD of channel is known complexity of the

Table 4 Number of complex multiplications for different receivers

CASE	OFDM	GFDM–ZF	GFDM–MMSE	GFDM–D-SIC	SVD–GFDM Rx (known SVD)	SVD–GFDM Rx (unknown SVD)	BIDFT–GFDM joint processing	BIDFT–GFDM two-stage processing	DFT–GFDM
TI	8.9×10^3	4.19×10^5	8.8×10^7	3.2×10^6	4.09×10^5	6.8×10^9	3.7×10^6	5×10^5	4.2×10^5
WRAN	1.62×10^4	4.16×10^6	2.8×10^9	3.3×10^7	4.1×10^6	2.1×10^{11}	2.4×10^7	4.19×10^6	4.16×10^6

IET Commun., 2015, Vol. 9, Iss. 15, pp. 1829–1841
© The Institution of Engineering and Technology 2015

Table 5 Values of *N* and *M* for different application scenarios [19]

(*N*, *M*)	TI (128, 5)	WRAN (16, 127)

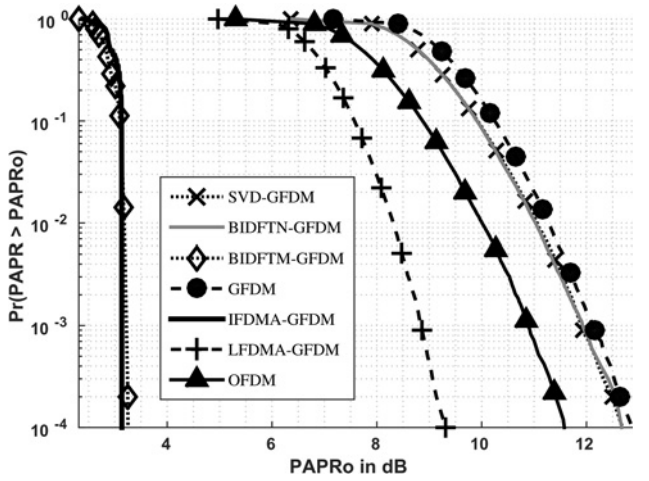

Fig. 9 *Complementary cumulative distribution function (empirical) of PAPR for GFDM for N = 128, M = 5, ROF = 0.5 (RRC) and Q = 4*

receiver is comparable with GFDM–ZF. Hence, SVD-based precoding can be used in cases when channel is constant for multiple transmit instances. Performance of BIDFT*N* precoding is found to be better than GFDM–ZF and GFDM–D-SIC. Two-stage BIDFT*N* precoded GFDM has complexity similar to GFDM–ZF and lesser than GFDM–D-SIC as well as gives lower PAPR. Hence, two-stage BIDFT*N* precoded GFDM should be preferred than GFDM–ZF. BIDFT*M* precoded as well as DFT precoded GFDM receivers which require complexity similar to GFDM–ZF performs much better than even GFDM–MMSE receiver under FSFC. Apart from this, BIDFT*M* and DFT precoded GFDM reduces PAPR significantly. Precoded GFDM system proposed in this paper can give better BER performance than GFDM system with no increase in complexity with the added advantage of decreased PAPR. It can be concluded that BIDFT*M* precoded GFDM should be preferred to other precoding schemes as it gives better BER performance than other precoded and uncoded receivers and decreases PAPR significantly without any increase in complexity.

7 References

1 Sesia, S., Toufik, I., Baker, M.: 'LTE – the UMTS long term evolution: from theory to practice' (John Wiley & Sons, Hoboken, NJ, USA, 2011)
2 Holma, H., Toskala, A.: 'LTE for UMTS: evolution to LTE-advanced' (John Wiley & Sons, Hoboken, NJ, USA, 2010)
3 Wunder, G., Kasparick, M., ten Brink, S., *et al.*: '5GNOW: challenging the LTE design paradigms of orthogonality and synchronicity'. 2013 IEEE Vehicular Technology Conf. (VTC Spring), Dresden, Germany, June 2013, pp. 1–5
4 METIS: 'Scenarios, requirement and KPIs for 5G mobile and wireless system', METIS, April 2013, vol. ICT-317669, no. D1.1
5 Santhi, K., Srivastava, V., Senthil Kumaran, G., Butare, A.: 'Goals of true broad band's wireless next wave (4G–5G)'. 2003 IEEE Vehicular Technology Conf., (VTC Fall), FL, USA, October 2003, pp. 2317–2321
6 Fettweis, G.: 'A 5G wireless communications vision', *Microw. J.*, 2012, **55**, (12), pp. 24–36
7 Wunder, G., Jung, P., Kasparick, M., *et al.*: '5GNOW: non-orthogonal, asynchronous waveforms for future mobile applications', *IEEE Commun. Mag.*, 2014, **52**, (2), pp. 97–105
8 Banelli, P., Buzzi, S., Colavolpe, G., Modenini, A., Rusek, F., Ugolini, A.: 'Modulation formats and waveforms for 5G networks: Who will be the heir of OFDM?: an overview of alternative modulation schemes for improved spectral efficiency', *IEEE Signal Process. Mag.*, 2014, **31**, (6), pp. 80–93
9 Bellanger, M.: 'Physical layer for future broadband radio systems'. 2010 IEEE Radio and Wireless Symp. (RWS), New Orleans, USA, January 2010, pp. 436–439
10 Cherubini, G., Eleftheriou, E., Olcer, S.: 'Filtered multitone modulation for very high-speed subscriber lines', *IEEE J. Sel. Areas Commun.*, 2002, **20**, (5), pp. 1016–1028
11 Saltzberg, B.: 'Performance of an efficient parallel data transmission system', *IEEE Trans. Commun. Technol.*, 1967, **15**, (6), pp. 805–811
12 Sandberg, S.D., Tzannes, M.A.: 'Overlapped discrete multitone modulation for high speed copper wire communications', *IEEE J. Sel. Areas Commun.*, 1995, **13**, (9), pp. 1571–1585
13 Swindlehurst, A., Ayanoglu, E., Heydari, P., Capolino, F.: 'Millimeter-wave massive MIMO: the next wireless revolution?', *IEEE Commun. Mag.*, 2014, **52**, (9), pp. 56–62
14 Michailow, N., Gaspar, I., Krone, S., Lentmaier, M., Fettweis, G.: 'Generalized frequency division multiplexing: analysis of an alternative multi-carrier technique for next generation cellular systems'. 2012 Int. Symp. on Wireless Communication Systems (ISWCS), Ilmenau, Germany, August 2012, pp. 171–175
15 Vakilian, V., Wild, T., Schaich, F., ten Brink, S., Frigon, J.-F.: 'Universal-filtered multi-carrier technique for wireless systems beyond LTE'. 2013 IEEE Globecom Workshops, Atlanta, USA, December 2013, pp. 223–228
16 Chang, R.: 'High-speed multichannel data transmission with bandlimited orthogonal signals', *Bell Syst. Tech. J.*, 1966, **45**, pp. 1775–1796
17 Schaich, F., Wild, T., Chen, Y.: 'Waveform contenders for 5G – suitability for short packet and low latency transmissions'. 2014 IEEE Vehicular Technology Conf. (VTC Spring), Seoul, Korea, May 2014, pp. 1–5
18 Fettweis, G., Krondorf, M., Bittner, S.: 'GFDM – generalized frequency division multiplexing'. 2009 IEEE Vehicular Technology Conf. VTC Spring, Glasgow, Scotland, April 2009, pp. 1–4
19 Michailow, N., Matthe, M., Gaspar, I., *et al.*: 'Generalized frequency division multiplexing for 5th generation cellular networks', *IEEE Trans. Commun.*, 2014, **62**, (9), pp. 3045–3061
20 Matthe, M., Michailow, N., Gaspar, I., Fettweis, G.: 'Influence of pulse shaping on bit error rate performance and out of band radiation of generalized frequency division multiplexing'. 2014 IEEE Int. Conf. on Communications Workshops (ICC), Sydney, Australia, June 2014, pp. 43–48
21 Gaspar, I., Michailow, N., Navarro, A., Ohlmer, E., Krone, S., Fettweis, G.: 'Low complexity GFDM receiver based on sparse frequency domain processing'. 2013 IEEE Vehicular Technology Conf. (VTC Spring), Dresden, Germany, June 2013, pp. 1–6
22 Alves, B.M., Mendes, L.L., Guimaraes, D.A., Gaspar, I.S.: 'Performance of GFDM over frequency-selective channels'. Int. Workshop on Telecommunications, Santa Rita do Sapuca, Brazil, 6–9 May 2013
23 Michailow, N., Krone, S., Lentmaier, M., Fettweis, G.: 'Bit error rate performance of generalized frequency division multiplexing'. 2012 IEEE Vehicular Technology Conf. (VTC Fall), Quebec City, Canada, September 2012, pp. 1–5
24 Datta, R., Michailow, N., Lentmaier, M., Fettweis, G.: 'GFDM interference cancellation for flexible cognitive radio PHY design'. 2012 IEEE Vehicular Technology Conf. (VTC Fall), Quebec City, Canada, September 2012, pp. 1–5
25 Slimane, S.: 'Peak-to-average power ratio reduction of OFDM signals using pulse shaping'. 2000 IEEE Global Telecommunications Conf., San Francisco, USA, November 2000, pp. 1412–1416
26 Michailow, N., Fettweis, G.: 'Low peak-to-average power ratio for next generation cellular systems with generalized frequency division multiplexing'. 2013 Int. Symp. on Intelligent Signal Processing and Communications Systems (ISPACS), Okinawa, Japan, November 2013, pp. 651–655
27 Proakis, J.G., Salehi, M.: 'Digital communication' (McGraw-Hill, New York, USA, 2008), ch. 13
28 Strang, G.: 'Linear algebra and its applications' (Brooks Cole, CA, USA, 1988)
29 Trapp, G.E.: 'Inverses of circulant matrices and block circulant matrices', *Kyungpook Math. J.*, 1973, **13**, (1), pp. 11–20
30 Simon, M.K., Alouini, M.-S.: 'Digital communication over fading channels' (John Wiley & Sons, Hoboken, NJ, USA, 2005), vol. 95
31 Chung, S.T., Goldsmith, A.: 'Degrees of freedom in adaptive modulation: a unified view', *IEEE Trans. Commun.*, 2001, **49**, (9), pp. 1561–1571
32 De Mazancourt, T., Gerlic, D.: 'The inverse of a block-circulant matrix', *IEEE Trans. Antennas Propag.*, 1983, **31**, (5), pp. 808–810
33 Falconer, D.D.: 'Linear precoding of OFDMA signals to minimize their instantaneous power variance', *IEEE Trans. Commun.*, 2011, **59**, (4), pp. 1154–1162
34 Myung, H., Lim, J., Goodman, D.: 'Peak-to-average power ratio of single carrier FDMA signals with pulse shaping'. 2006 IEEE Int. Symp. on Personal, Indoor and Mobile Radio Communications (PIMRC), Helsinki, Finland, September 2006, pp. 1–5
35 Blahut, R.E.: 'Fast algorithms for signal processing' (Cambridge University Press, Cambridge, UK, 2010)

© The Institution of Engineering and Technology 2015

Copyright of IET Communications is the property of Institution of Engineering & Technology and its content may not be copied or emailed to multiple sites or posted to a listserv without the copyright holder's express written permission. However, users may print, download, or email articles for individual use.